THE ASTROPHYSICAL JOURNAL, 453:890–905, 1995 November 10

PITCH ANGLE DIFFUSION COEFFICIENT IN AN EXTENDED QUASI-LINEAR THEORY

C. K. NG[1,2] AND D. V. REAMES
Laboratory for High Energy Astrophysics, Code 661, NASA/Goddard Space Flight Center, Greenbelt, MD 20771
Received 1995 March 13; accepted 1995 May 19

ABSTRACT

Using an extended quasi-linear theory that takes account of the distribution of medium-scale background interplanetary magnetic field, we calculate the pitch angle diffusion coefficients of interplanetary energetic ions, for a slab turbulence model consisting of a superposition of parallel and antiparallel transverse R and L waves. Our results show that the background variation broadens the resonance function significantly at pitch angles near 90°, so that protons down to $\approx$25 keV interact with hydromagnetic waves at all pitch angles, and the steepening of the magnetic field power spectrum in the dissipation range does not result in a resonance gap or infinite scattering mean free path.

Subject headings: acceleration of particles — diffusion — interplanetary medium — MHD — Sun: particle emission

1. INTRODUCTION

For many decades the standard quasi-linear theory (SQLT) of wave-particle interaction has provided a theoretical basis for the transport and acceleration of energetic charged particles in various astrophysical plasmas, e.g., solar flares, interplanetary space, and the interstellar medium (e.g., Fisk 1979; Lee 1983; Schlickeiser 1992; Völk 1975). Theory and observation are most closely linked in the study of the interplanetary acceleration and transport of "solar" energetic particles (SEPs) (e.g., Reames, 1993, 1994). This is because (*a*) on detection, SEPs typically have interacted with waves or fluctuations only over a comparatively small distance and in a comparatively short interval of time, making it easier to identify causes and effects, and (*b*) there is a wealth of increasingly sophisticated in situ spacecraft observations on both SEPs and the properties of the solar wind since the early 1960s. Studies on SEPs therefore have great relevance to the wider astrophysical community because they subject the widely applied transport and acceleration theories to tests that are often not possible elsewhere.

SQLT has a fundamental difficulty that manifests itself most clearly at $\mu = 0$, where μ denotes the cosine of the particle pitch angle, in the magnetostatic approximation (Klimas & Sandri 1971). The extensive work in the 1970s addressed to this and related issues was reviewed in Fisk (1979). As pointed out by Fisk, the various nonlinear theories (e.g., Völk 1973, 1975; Goldstein 1976; Jones, Kaiser, & Birmingham 1973; Jones, Birmingham, & Kaiser 1978) constructed to overcome the theoretical difficulty of SQLT at $\mu = 0$, ironically tended to increase the discrepancy between the mean free paths predicted by SQLT and those inferred from SEP observations (Palmer 1982). The situation has taken another ironic turn in recent years as a result of the realization of the importance of the thermal damping of ion-cyclotron and electron-cyclotron waves, first pointed out in this context by Davila & Scott (1984a, b) (see also Miller & Steinacker 1992; Achatz et al. 1993). Including the steep fluctuation spectrum in the dissipation range of wavenumbers in SQLT resulted in a region of weak scattering or resonance gap and correspondingly very long or infinite scattering mean free paths (Smith, Bieber, & Matthaeus 1990; Achatz et al. 1993). These authors pointed out that this was actually a significant step forward, for nonlinear or other effects may now provide the additional scattering to lower the theoretical mean free paths to the values inferred from SEP observations. Schlickeiser & Achatz (1993a, b) and Bieber et al. (1994) have recently addressed this issue by considering resonance broadening that results from thermal wave damping and dynamical turbulence. In this paper, we consider a different resonance broadening mechanism that results from taking account of the medium scale magnetic field fluctuation.

Let us look briefly at the assumptions and procedures in SQLT (e.g., Hall & Sturrock 1967; Kennel & Engelmann 1966; Kulsrud & Pearce 1969; Achatz, Steinacker, & Schlickeiser 1991; Steinacker & Miller 1992; Jaekel & Schlickeiser 1992). The momentum transport coefficients or Fokker-Planck coefficients are derived in SQLT by summing the perturbations to the particle momentum resulting from *resonant* interactions between the particles and the fluctuating electromagnetic fields. These perturbations are calculated using an unperturbed particle orbit in the *mean* magnetic field, it being assumed that these perturbations, integrated over a time interval of coherent resonant wave-particle interaction, are so small as to produce negligible changes to the particle orbit. It is well known that in the magnetostatic approximation, this prescription runs into difficulty when the parallel particle speed vanishes and the assumed unperturbed orbit becomes unreliable for calculating the perturbations. In the case of the slab model of transverse fluctuations, in which the wave fields or the correlation functions of the fluctuations vary with only one coordinate z parallel to the mean field, SQLT predicts that the diffusion coefficient $D_{\mu\mu}$ vanishes at $\mu = 0$, if the magnetostatic approximation is made, and at $\mu = v_A/v$ if the transverse waves are hydromagnetic, parallel, and unidirectional. For low-energy ions, steepening of the wave spectrum near the proton cyclotron frequency accentuates this to a finite region in which $D_{\mu\mu}$ is very small or vanishes (resonance gap), even in the presence of counter-streaming waves. Besides, observation indicates that $\approx$90% of the waves are propagating

[1] NRC/NAS Senior Research Associate.
[2] On leave from Royal Melbourne Institute of Technology, Melbourne, Australia.

antisunward relative to the solar wind plasma (Denskat & Neubauer 1982). Thus, SQLT predicts very large or infinite mean free paths.

An important assumption in SQLT is the constant background magnetic field. However, observed time series of the interplanetary magnetic field (IMF) show fluctuations on a broad range of timescales. At ~ 1 AU heliocentric distance, the standard deviations of the fluctuations in the vector magnetic field and in the fluctuations in the magnetic field magnitude in hour-long intervals vary considerably from hour to hour, averaging to $\approx 30\%$ and $\approx 8\%$ of the average field magnitude (Denskat & Neubauer 1983). The hourly averaged field magnitude usually differs from hour to hour by approximately 2%–10% (e.g., King 1975). Well-connected SEP events at ~ 1 MeV nucleon^{-1} often takes 5–10 hours to rise to the maximum and last for more than a day, whereas the proton gyroperiod is about 12 s in a typical 5 nT field at 1 AU heliocentric distance, decreasing toward the Sun. Thus, on a timescale long compared to the gyroperiod but short compared to the duration of an SEP event, the background goes through significant variations in both direction and magnitude, making the use of unperturbed orbits in an assumed constant background rather dubious.

The effect of the varying background magnetic field $\boldsymbol{B}'$ was considered by Jones et al. (1978) in their nonlinear partial average theory, in which particle orbits are followed in magnetic fields averaged over subsets of an ensemble of random static magnetic fields, and the results were averaged over all subsets. Their results compared favorably with those derived from Monte Carlo simulations of particle orbits in the full ensemble (Kaiser, Birmingham, & Jones 1978). A nonlinear analytical calculation without assuming unperturbed orbits was carried out by Goldstein (1976) in the magnetostatic approximation. Völk (1975) took account heuristically of the effect of magnetic field magnitude fluctuation on the particle's pitch angle in terms of a nonlinear integral equation. These nonlinear formulations require elaborate computer simulations, solution to a complicated system of differential equations, or solution to a nonlinear integral equation, respectively.

In this paper, we present a heuristic extension to SQLT that takes account of the medium-scale fluctuations in the background in an approach that has some similarities to the nonlinear approaches of Jones et al. (1978) and Völk (1975). Like Jones et al., we calculate the result for each member of a statistical distribution of the background magnetic fields and then average the calculated results over this distribution. However, whereas Jones et al.'s partially averaged magnetic fields exhibit magnitude variation, our backgrounds are approximated by magnetic fields with constant magnitude, allowing the use of zero-order unperturbed particle orbits in the quasi-linear calculation. Nevertheless, we do take heuristic account of the effects of the slow adiabatic variation in the background field magnitude $|\boldsymbol{B}'|$ on the particle's pitch-angle cosine μ' relatvie to $\boldsymbol{B}'$. As the particle responds to the varying field magnitudes, the approximate conservation of the particle's magnetic moment causes its μ' to oscillate, even across the resonance gap (Völk 1975). Instead of using a nonlinear treatment like Völk's, we take account of this by averaging over the *nominal* particle gyrophase and the azimuth and magnitude of the background magnetic field; this effectively includes averaging over the range of uncertainty of μ' (see § 2.2).

Our medium-scale background magnetic fields are specified in the form $\boldsymbol{B}' \equiv \boldsymbol{B}_0 + \Delta\boldsymbol{B}$, where $\boldsymbol{B}_0$ is the mean, $\Delta\boldsymbol{B}$ is a constant vector perpendicular to $\boldsymbol{B}_0$, and we assume $(\Delta B)^2/B_0^2 \ll 1$. For fluctuations at the higher frequencies in gyroresonance with SEPs, we assume for simplicity the slab model, consisting of a superposition of transverse electromagnetic circularly polarized R and L waves propagating parallel and antiparallel to the mean magnetic field $\boldsymbol{B}_0$. We use unperturbed orbits in each constant background magnetic field to calculate the transport coefficients for that background using the method of SQLT and then average the coefficients over the distribution of all possible backgrounds. We apply our considerations mainly to $\lesssim 20$ MeV nucleon^{-1} interplanetary ions and present detailed calculations only for $D_{\mu\mu}$, the diffusion coefficient in μ-space. Our calculations show that for protons down to ≈ 25 keV, inclusion of the fluctuating background significantly broadens the resonance range of wavenumbers near $|\mu| = 0$, so that the resonance gap does not exist for these energetic ions in interplanetary space, even when the wave spectrum is cut off above a frequency close to but below the proton gyrofrequency.

The plan of the rest of this paper is as follows. In § 2 we extend the SQLT procedure to give a formal derivation of the transport equation from the Vlasov equation. The effect of medium-scale variation in $|\boldsymbol{B}'|$ is discussed. The transport coefficients are derived in terms of a sum over the contribution of each wave mode, with each contribution expressed as an integral on the product of the differential wave intensity and the resonance function for that wave mode. Each resonance function is in turn given as an integral that may be evaluated numerically. In § 3 we present and interpret the numerically calculated resonance functions. We use the cold plasma dispersion relation, which is a reasonable approximation as the resonance functions peak at hydromagnetic frequencies. In § 4, we present the numerical results on $D_{\mu\mu}$. The paper closes with a summary and discussion in § 5.

2. EXTENDED QUASI-LINEAR THEORY

2.1. *Transport Equation in Slab Turbulence*

For simplicity, we assume the slab turbulence in which the field fluctuation is taken to be a superposition of transverse electromagnetic circularly polarized plane waves propagating parallel and antiparallel to the constant *mean* magnetic field $\boldsymbol{B}_0$. The mean electric field is assumed to be zero. We take advantage of the symmetry of the Fourier transforms of real quantities and the relation $\omega^\sigma(k) = -\omega^\sigma(-k)$, where $\omega^\sigma(k)$ denotes the angular frequency of the circularly polarized σ-mode, to restrict the (parallel) wavenumber k to positive values for $\sigma = R^+, L^-$, and negative values for $\sigma = R^-, L^+$. Here R and L denote right and left polarization, and $+$ and $-$ denote propagation away from ($\hat{z}$) and toward ($-\hat{z}$) the Sun along the mean IMF. We shall adopt the following convention: $\omega > (<)\ 0$ corresponds to right (left) polarization, and $\omega/k > (<)\ 0$ corresponds to antisunward (sunward) propagation. If $\boldsymbol{B}_0$ is parallel to $\hat{z}$, then $k > (<)\ 0$ corresponds to left (right) helicity; otherwise $k > (<)\ 0$ corresponds to the right (left) helicity. By helicity here, we mean the left- or right-hand spatial structure of the wave. The convention described above allows the dispersion relations for the four different wave modes to be graphed on distinct quadrants of the k-ω plane. (In Ng & Reames [1994]), the R, L labels refer to the helicity, whereas here they refer to the polarization.) When the SQLT cyclotron resonance

condition

$$\omega - kv_{\parallel} = -\Omega_0/\gamma \tag{2.1}$$

is also plotted on the same graph, the resonant wave modes and resonant wavenumbers can be read directly off the graph (Fig. 1). Here $v_{\parallel}$ is the parallel velocity of the particle, γ is its Lorentz factor, and Ω_0 is its cyclotron frequency in the mean field $\boldsymbol{B}_0$.

The spectrum of interplanetary magnetic fluctuation is observed to be approximately a power law with index ≈ 1.5–1.7 in the inertial range (e.g., Roberts, Goldstein, & Klein 1990). We divide the wavenumber space into a high k-range with wavelengths $\lesssim 5 \times 10^{-4}$ AU, and a low k-range with wavelengths from $\approx 1 \times 10^{-2}$ AU to $\approx 1 \times 10^{-1}$ AU. We lump together all the medium-scale larger amplitude waves in the low k-range into a slowly varying transverse component, whose principal effect is to combine with the mean field $\boldsymbol{B}_0$ to provide a slowly varying background magnetic field, whereas the high k-range is selected to resonate with the energetic particles under consideration. This separation of length scales means we can only consider particles whose parallel velocities are sufficiently small. In the extended quasi-linear theory (EQLT), we specify the wave spectrum in the high k-range but only the probability distribution of the integrated transverse component of the medium-scale fluctuation.

The differential wave intensities in the high range $(k_1^{\sigma}, k_2^{\sigma})$ contribute to the small-scale magnetic and electric field fluctuations $\delta\boldsymbol{B}(z, t)$ and $\delta\boldsymbol{E}(z, t)$. Thus, we have

$$\delta\boldsymbol{B}(z, t) = \Re \sum_{\sigma} \int_{k_1^{\sigma}}^{k_2^{\sigma}} \frac{dk}{2\pi} \exp\left[ikz - i\omega^{\sigma}(k)t\right] \delta\bar{B}^{\sigma}(k)(\hat{\boldsymbol{x}} + i\hat{\boldsymbol{y}}) , \tag{2.2}$$

$$\delta\boldsymbol{E}(z, t) = \Re \sum_{\sigma} \int_{k_1^{\sigma}}^{k_2^{\sigma}} \frac{dk}{2\pi} \exp\left[ikz - i\omega^{\sigma}(k)t\right] \frac{\omega^{\sigma}(k)}{kc} \delta\bar{B}^{\sigma}(k)(\hat{\boldsymbol{y}} - i\hat{\boldsymbol{x}}) . \tag{2.3}$$

In the above equations, $\Re$ means the real part, $\delta\bar{B}^{\sigma}(k)$ denotes wave complex wave amplitude of the circularly polarized σ-mode, and $\hat{\boldsymbol{x}}$, $\hat{\boldsymbol{y}}$, and $\hat{\boldsymbol{z}}$ denote unit vectors parallel to the fixed Ox, Oy, and Oz-axes, respectively, with $\hat{\boldsymbol{z}}$ parallel to $\boldsymbol{B}_0$. The sum is taken over all four wave modes. The limits of integration are taken as follows. For $\sigma = R^+, L^-$, we take $(k_1^{\sigma}, k_2^{\sigma}) = (k_{\min}, k_{\max})$; for $\sigma = R^-, L^+$, we take $(k_1^{\sigma}, k_2^{\sigma}) = (-k_{\max}, -k_{\min})$, where $0 < k_{\min} < k_{\max}$.

We give below a formal derivation of the transport equation for energetic charged particles following SQLT (Hall & Sturrock 1967; Kennel & Engelmann 1966; Kulsrud & Pearce 1969), but taking account heuristically of the medium-scale fluctuations on the zero-order particle orbit. We start with the Vlasov equation

$$\left(\frac{\partial}{\partial t} + \boldsymbol{v} \cdot \frac{\partial}{\partial \boldsymbol{r}} + \boldsymbol{F} \cdot \frac{\partial}{\partial \boldsymbol{p}}\right) f(\boldsymbol{r}, \boldsymbol{p}, t) = 0 , \tag{2.4}$$

where

$$\boldsymbol{F} = \boldsymbol{F}_0 + \Delta\boldsymbol{F} + \delta\boldsymbol{F} , \qquad \boldsymbol{F}_0 = (q/c)\boldsymbol{v} \times \boldsymbol{B}_0 , \qquad \Delta\boldsymbol{F} = q\,\Delta\boldsymbol{E} + (q/c)\boldsymbol{v} \times \Delta\boldsymbol{B} , \qquad \delta\boldsymbol{F} = q\,\delta\boldsymbol{E} + (q/c)\boldsymbol{v} \times \delta\boldsymbol{B} . \tag{2.5}$$

In the above, f denotes the particle phase space density, $\boldsymbol{F}$ is the Lorentz force, $\boldsymbol{r}$ is the position vector, t is time, $\boldsymbol{p}$ is the particle momentum, $\boldsymbol{v}$ is the particle velocity, q is the particle's charge, and c is the speed of light. Denoting averages over realizations of the small- and medium-scale fields by the subscripted angle brackets $\langle\ \rangle_{\delta}$ and $\langle\ \rangle_{\Delta}$, respectively, we have

$$\langle\Delta\boldsymbol{F}\rangle_{\Delta} = \langle\Delta\boldsymbol{B}\rangle_{\Delta} = \langle\Delta\boldsymbol{E}\rangle_{\Delta} = \boldsymbol{0} , \qquad \langle\delta\boldsymbol{F}\rangle_{\Delta} = \langle\delta\boldsymbol{B}\rangle_{\delta} = \langle\delta\boldsymbol{E}\rangle_{\delta} = \boldsymbol{0} , \qquad \langle\langle\boldsymbol{B}\rangle_{\delta}\rangle_{\Delta} \equiv \langle\langle\boldsymbol{B}_0 + \Delta\boldsymbol{B} + \delta\boldsymbol{B}\rangle_{\delta}\rangle_{\Delta} = \boldsymbol{B}_0 . \tag{2.6}$$

During its *resonant* interaction with $\delta\boldsymbol{B}$ and $\delta\boldsymbol{E}$ of the short-wavelength transverse waves, the particle senses the larger but more slowly varying $\Delta\boldsymbol{B}$ and $\Delta\boldsymbol{E}$ of the medium-scale nonresonant waves as part of the local background. We take account of this heuristically by calculating the particle's zero-order orbit in the effective local background magnetic field $\boldsymbol{B}_0 + \Delta\boldsymbol{B}$, approximated by a constant and neglecting the background electric field $\Delta\boldsymbol{E}$. The resulting particle transport coefficients due to quasi-linear resonant wave-particle interaction are averaged over an assumed axisymmetric probability distribution of $\Delta\boldsymbol{B}$ with zero mean. The details are given below.

Assuming that $\delta B \ll \Delta B \ll B_0$, and so $\delta F \ll \Delta F \ll F_0$, we introduce

$$f = \langle f\rangle + \Delta f + \delta f , \tag{2.7}$$

where

$$\langle\delta f\rangle_{\delta} = \langle\Delta f\rangle_{\Delta} = 0 , \tag{2.8}$$

$\langle f\rangle \equiv \langle\langle f\rangle_{\delta}\rangle_{\Delta}$, and $|\delta f|, |\Delta f| \ll f$. Following the usual quasi-linear derivation, we substitute equations (2.5) and (2.7) in equation (2.4) and average over the small-scale fluctuations. This yields

$$\left[\frac{\partial}{\partial t} + \boldsymbol{v} \cdot \frac{\partial}{\partial \boldsymbol{r}} + (\boldsymbol{F}_0 + \Delta\boldsymbol{F}) \cdot \frac{\partial}{\partial \boldsymbol{p}}\right]\langle f\rangle_{\delta} = -\frac{\partial}{\partial \boldsymbol{p}} \cdot \langle\delta\boldsymbol{F}\delta f\rangle_{\delta} . \tag{2.9}$$

Subtracting this from equation (2.4) and neglecting the bilinear terms yields

$$\left[\frac{\partial}{\partial t} + \boldsymbol{v} \cdot \frac{\partial}{\partial \boldsymbol{r}} + (\boldsymbol{F}_0 + \Delta\boldsymbol{F}) \cdot \frac{\partial}{\partial \boldsymbol{p}}\right]\delta f = -\delta\boldsymbol{F} \cdot \frac{\partial}{\partial \boldsymbol{p}}\langle f\rangle_{\delta} , \tag{2.10}$$

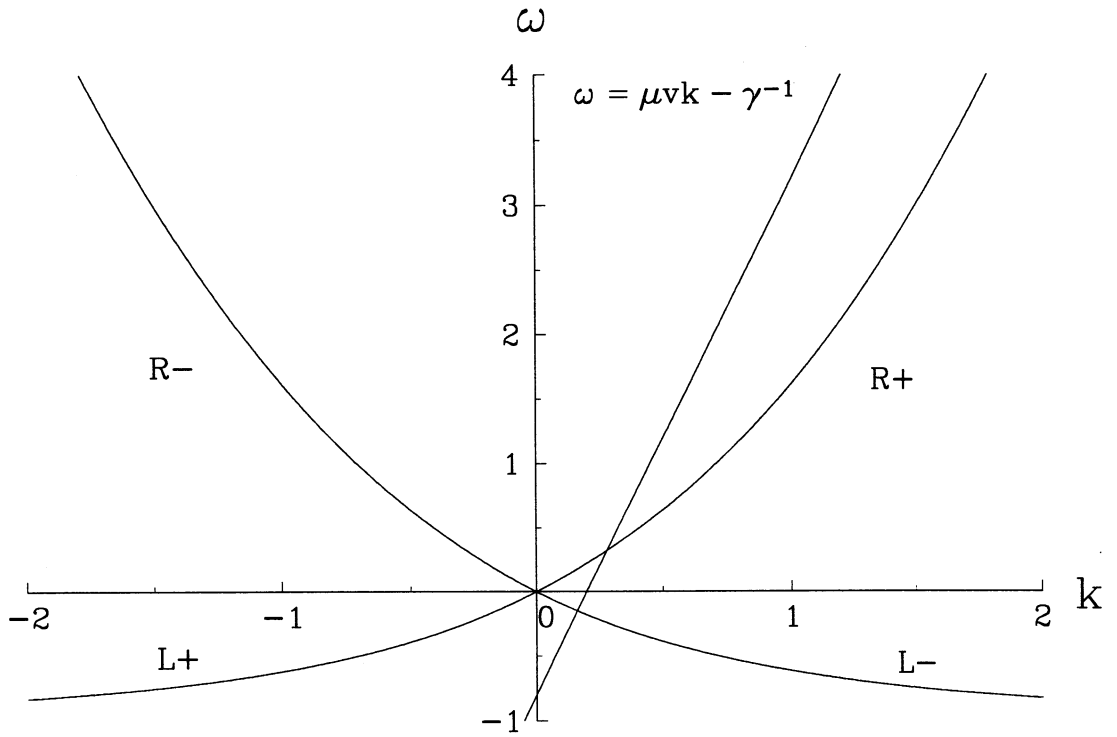

FIG. 1.—The normalized cold plasma dispersion relations for parallel and antiparallel $R\pm$ and $L\pm$ waves, and the normalized cyclotron resonance condition. See eq. (3.1) for the definition of the normalized quantities ω, k, and v.

the formal solution to which is

$$\delta f(\boldsymbol{r}, \boldsymbol{p}, t) = -\int_0^{\tau_\delta} d\tau \left(\delta \boldsymbol{F} \cdot \frac{\partial}{\partial \boldsymbol{p}} \langle f \rangle_\delta \right)_{\boldsymbol{r}(t-\tau), \boldsymbol{p}(t-\tau), t-\tau}, \tag{2.11}$$

where the parentheses indicate that the expression within is to be evaluated at the earlier time $t - \tau$ and at the point $[\boldsymbol{r}(t - \tau), \boldsymbol{p}(t - \tau)]$ in phase space on the unperturbed particle orbit. The timescale τ_δ of coherent wave-particle interaction is taken as the upper limit of the integral. We calculate the unperturbed orbit in the local background magnetic field $\boldsymbol{B}' \equiv \boldsymbol{B}_0 + \Delta \boldsymbol{B}$ instead of the mean field $\boldsymbol{B}_0$ as in SQLT. Since the timescale τ_Δ of the medium-scale fluctuation $\Delta \boldsymbol{B}$ is large compared to τ_δ, we approximate $\Delta \boldsymbol{B}$ by a constant, characterizing its statistical fluctuation by a probability distribution with zero mean and finite range.

Substituting equation (2.11) in equation (2.9) yields the integro-differential equation

$$\left[\frac{\partial}{\partial t} + \boldsymbol{v} \cdot \frac{\partial}{\partial \boldsymbol{r}} + (\boldsymbol{F}_0 + \Delta \boldsymbol{F}) \cdot \frac{\partial}{\partial \boldsymbol{p}} \right] \langle f \rangle_\delta = -\frac{\partial}{\partial \boldsymbol{p}} \cdot \int_0^{\tau_\delta} d\tau \left\langle \delta \boldsymbol{F}[\boldsymbol{r}(t), \boldsymbol{p}(t), t] \delta \boldsymbol{F}(\boldsymbol{r}', \boldsymbol{p}', t') \cdot \frac{\partial \langle f \rangle_\delta(\boldsymbol{r}', \boldsymbol{p}', t')}{\partial \boldsymbol{p}'} \right\rangle_\delta, \tag{2.12}$$

where $\boldsymbol{r}' \equiv \boldsymbol{r}(t - \tau)$, $\boldsymbol{p}' \equiv \boldsymbol{p}'(t - \tau)$, and $t' \equiv t - \tau$. We assume $\tau_{\Omega'} \ll \tau_\delta \ll \tau_f$, where $\tau_{\Omega'}$ denotes the gyroperiod and τ_f denotes the timescale of variation of f_δ. Taylor expanding the last momentum derivative about $[\boldsymbol{r}(t), \boldsymbol{p}(t), t]$, we have

$$\frac{\partial \langle f \rangle_\delta(\boldsymbol{r}', \boldsymbol{p}', t')}{\partial \boldsymbol{p}'} = \frac{\partial \langle f \rangle_\delta}{\partial \boldsymbol{p}} - \left\{ \tau \frac{\partial^2 \langle f \rangle_\delta}{\partial t \, \partial \boldsymbol{p}} + [\boldsymbol{p}(t - \tau) - \boldsymbol{p}(t)] \cdot \frac{\partial^2 \langle f \rangle_\delta}{\partial \boldsymbol{p} \, \partial \boldsymbol{p}} + [\boldsymbol{r}(t - \tau) - \boldsymbol{r}(t)] \cdot \frac{\partial^2 \langle f \rangle_\delta}{\partial \boldsymbol{r} \, \partial \boldsymbol{p}} \right\} + \cdots, \tag{2.13}$$

where the derivatives of f on the right are evaluated at $[\boldsymbol{r}(t), \boldsymbol{p}(t), t]$. Assuming that the second derivatives of f are small enough such that terms beyond the first on the right can be neglected, we obtain the transport equation in the form of a diffusion or Fokker-Planck equation:

$$\left[\frac{\partial}{\partial t} + \boldsymbol{v} \cdot \frac{\partial}{\partial \boldsymbol{r}} + (\boldsymbol{F}_0 + \Delta \boldsymbol{F}) \cdot \frac{\partial}{\partial \boldsymbol{p}} \right] \langle f \rangle_\delta = \frac{\partial}{\partial \boldsymbol{p}} \cdot \int_0^{\tau_\delta} d\tau \langle \delta \boldsymbol{F}[\boldsymbol{r}(t), \boldsymbol{p}(t), t] \delta \boldsymbol{F}(\boldsymbol{r}', \boldsymbol{p}', t') \rangle_\delta \cdot \frac{\partial \langle f \rangle_\delta(\boldsymbol{r}, \boldsymbol{p}, t)}{\partial \boldsymbol{p}}. \tag{2.14}$$

We will average equation (2.14) over (*a*) one gyroperiod from t to $t + \tau_{\Omega'}$ following the unperturbed particle orbit (indicated by $\langle \ \rangle_{\tau_{\Omega'}}$), (*b*) all nominal gyrophase $\varphi_0 \equiv \varphi$ at time t about the *mean* magnetic field $\boldsymbol{B}_0$ (indicated by $\langle \ \rangle_\varphi$), and (*c*) all realizations of the medium-scale fluctuations (indicated by $\langle \ \rangle_\Delta$), to arrive at the final transport equation specified relative to the *mean* magnetic field. The particle's unperturbed orbit is given in § 2.2. Averaging equation (2.14) over one gyroperiod from t to $t + \tau_{\Omega'}$ following the unperturbed particle, assuming that $\langle f \rangle_\delta$ depends only on one space coordinate z, and noting that $\langle f \rangle_\delta$ and $\partial \langle f \rangle_\delta / \partial \boldsymbol{p}$ do not vary

significantly in one gyroperiod following the particle, we obtain

$$\frac{\partial\langle f\rangle_{\delta,\tau_{\Omega'}}}{\partial t}+\langle v_\parallel\rangle_{\tau_{\Omega'}}\frac{\partial\langle f\rangle_{\delta,\tau_{\Omega'}}}{\partial z}+\Omega'\left\langle\frac{\partial\langle f\rangle_\delta}{\partial\varphi'}\right\rangle_{\tau_{\Omega'}}+q\,\Delta\boldsymbol{E}\cdot\left\langle\frac{\partial\langle f\rangle_\delta}{\partial\boldsymbol{p}}\right\rangle_{\tau_{\Omega'}}$$
$$=\frac{\partial}{\partial\boldsymbol{p}}\cdot\int_0^{\tau_\delta}d\tau\langle\delta\boldsymbol{F}[\boldsymbol{r}(t),\boldsymbol{p}(t),t]\delta\boldsymbol{F}(\boldsymbol{r}',\boldsymbol{p}',t')\rangle_{\delta,\tau_{\Omega'}}\cdot\frac{\partial\langle f\rangle_{\delta,\tau_{\Omega'}}(\boldsymbol{r},\boldsymbol{p},t)}{\partial\boldsymbol{p}}\,,\quad(2.15)$$

where $\Omega'\equiv qB'/(\gamma mc)$ is the gyrofrequency, $\gamma=[1-(v/c)^2]^{-1/2}$, and $\langle\ \rangle_{\delta,\tau_{\Omega'}}\equiv\langle\langle\ \rangle_\delta\rangle_{\tau_{\Omega'}}$. Note that the gyroperiod-averaged $\langle f\rangle_{\delta,\tau_{\Omega'}}(\boldsymbol{r},\boldsymbol{p},t)$ is labeled by the start time t of the averaging interval $(t,t+\tau_{\Omega'})$, and by the space and momentum coordinates at t. Assuming that $\langle f\rangle_\delta$ is nearly gyrotropic about $\boldsymbol{B}'$, we drop the third term from the left of equation (2.15). The main effect of $\Delta\boldsymbol{E}$ is to produce an $E\times B$ drift velocity, whose z-component is only a fraction of the Alfvén speed, and whose component perpendicular to $\hat{\boldsymbol{z}}$ has no effect on wave-particle interaction, because the wave phase planes are also perpendicular to $\hat{\boldsymbol{z}}$. The fourth term can be shown to be small and so will be dropped. We assume that $\tau_\delta\ll\tau_\Delta\ll\tau_f$, where τ_f now denotes the timescale of the evolution of $\langle f\rangle_{\delta,\tau_{\Omega'}}$. Thus, the particles encounter essentially all realizations of $\Delta\boldsymbol{B}$ many times during a time interval of the order of τ_f, and we may average the above equation over all realizations of $\Delta\boldsymbol{B}$, and over all *nominal* gyrophase φ about $\boldsymbol{B}_0$, yielding

$$\frac{\partial\langle f\rangle}{\partial t}+\langle v_\parallel\rangle_{\tau_{\Omega'},\Delta,\varphi}\frac{\partial\langle f\rangle}{\partial z}=\frac{\partial}{\partial\boldsymbol{p}}\cdot\int_0^{\tau_\delta}d\tau\langle\delta\boldsymbol{F}[\boldsymbol{r}(t),\boldsymbol{p}(t),t]\delta\boldsymbol{F}(\boldsymbol{r}',\boldsymbol{p}',t')\rangle\cdot\frac{\partial\langle f\rangle(\boldsymbol{r},\boldsymbol{p},t)}{\partial\boldsymbol{p}}\,,\quad(2.16)$$

where $\langle\ \rangle\equiv\langle\ \rangle_{\delta,\tau_{\Omega'},\Delta,\varphi}$, and we have ignored the difference between $\langle f\rangle_{\delta,\tau_{\Omega'}}$ and $\langle f\rangle$ in the space derivative term. It should be pointed out that the average over the nominal gyrophase φ and the background fluctuation $\Delta\boldsymbol{B}$ includes averaging over the uncertainty range of μ' as a result of adiabatic oscillation in the nonresonant fluctuation of the background magnetic field magnitude (see below).

2.2. *Unperturbed Particle Orbit and Adiabatic Oscillation*

We specify first the unperturbed particle orbit in the approximation of a constant background magnetic field $\boldsymbol{B}'=\boldsymbol{B}_0+\Delta\boldsymbol{B}$ and then discuss how the uncertainty in μ' resulting from adiabatic oscillation is taken into account. In the constant magnetic field $\boldsymbol{B}'$, the position $\boldsymbol{r}(t)$ and velocity $\boldsymbol{v}(t)$ of a charged particle that passes through the origin with specified velocity at $t=0$ are given by

$$\boldsymbol{r}(t)=v'_{\parallel0}\,t\hat{\boldsymbol{z}}'+(v'_{\perp0}/\Omega')\{[\sin\varphi'_0-\sin(\varphi'_0-\Omega't)]\hat{\boldsymbol{x}}'+[\cos(\varphi'_0-\Omega't)-\cos\varphi'_0]\hat{\boldsymbol{y}}'\}\,,\quad(2.17)$$

$$\boldsymbol{v}(t)=v'_{\parallel0}\,\hat{\boldsymbol{z}}'+v'_{\perp0}\cos(\varphi'_0-\Omega't)\hat{\boldsymbol{x}}'+v'_{\perp0}\sin(\varphi'_0-\Omega't)\hat{\boldsymbol{y}}'\,,\quad(2.18)$$

where $v'_{\parallel0}$, $v'_{\perp0}$, and φ'_0 are, respectively, the velocity components parallel and perpendicular to $\boldsymbol{B}'$ and the gyrophase about $\boldsymbol{B}'$ at $t=0$. The gyrophase φ' is defined as the azimuth of the velocity projection perpendicular to $\boldsymbol{B}'$, measured anticlockwise from the Ox' axes. The unit vector $\hat{\boldsymbol{z}}'$ is chosen parallel to $\boldsymbol{B}'$, while $\hat{\boldsymbol{x}}'$ and $\hat{\boldsymbol{y}}'$ are defined by $\hat{\boldsymbol{x}}':=\hat{\boldsymbol{z}}\times\hat{\boldsymbol{z}}'/|\hat{\boldsymbol{z}}\times\hat{\boldsymbol{z}}'|$, $\hat{\boldsymbol{y}}':=\hat{\boldsymbol{z}}'\times\hat{\boldsymbol{x}}'$, respectively. The primed unit vectors are related to the unprimed unit vectors as follows:

$$\begin{bmatrix}\hat{\boldsymbol{x}}'\\ \hat{\boldsymbol{y}}'\\ \hat{\boldsymbol{z}}'\end{bmatrix}=\begin{bmatrix}-\sin\phi_B & \cos\phi_B & 0\\ -b_0\cos\phi_B & -b_0\sin\phi_B & b_\perp\\ b_\perp\cos\phi_B & b_\perp\sin\phi_B & b_0\end{bmatrix}\begin{bmatrix}\hat{\boldsymbol{x}}\\ \hat{\boldsymbol{y}}\\ \hat{\boldsymbol{z}}\end{bmatrix},\quad(2.19)$$

where $b_\perp=|\Delta\boldsymbol{B}|/B'$, $b_0=B_0/B'$, $B_0=|\boldsymbol{B}_0|$, $B'=|\boldsymbol{B}'|$, and ϕ_B is the azimuth of $\Delta\boldsymbol{B}$ measured anticlockwise from the Ox axis. Note that $b_\perp^2+b_0^2=1$. The relationship between the unprimed and primed coordinate systems and the definitions of the *nominal* gyrophase φ and the magnetic azimuth ϕ_B are illustrated in Figure 2. The parallel and perpendicular velocity components at time $t=0$ in the two systems are related by

$$v'_{\perp0}\cos\varphi'_0=v_{\perp0}\sin(\varphi_0-\phi_B)\,,$$
$$v'_{\perp0}\sin\varphi'_0=b_\perp v_{\parallel0}-b_0v_{\perp0}\cos(\varphi_0-\phi_B)\,,$$
$$v'_{\parallel0}=b_0v_{\parallel0}+b_\perp v_{\perp0}\cos(\varphi_0-\phi_B)\,.\quad(2.20)$$

Using equations (2.19) and (2.20) in equation (2.18), we may express the velocity projections parallel and perpendicular to the *mean* magnetic field $\boldsymbol{B}_0$ as

$$\boldsymbol{v}_\parallel(t)=\{v_{\parallel0}+b_\perp v_{\perp0}[\cos(\phi_B-\varphi_0)-\cos(\Omega't+\phi_B-\varphi_0)]-b_\perp^2v_{\parallel0}[1-\cos(\Omega't)]+O(b_\perp^3)\}\hat{\boldsymbol{z}}\,,\quad(2.21)$$

and

$$\boldsymbol{v}_\perp(t)\equiv\Re[v_\perp(t)\,e^{i\varphi(t)}(\hat{\boldsymbol{x}}-i\hat{\boldsymbol{y}})]$$
$$=\Re[[\{v_{\perp0}\,e^{i(\varphi_0-\Omega't)}+b_\perp v_{\parallel0}(e^{i\phi_B}-e^{i(\phi_B-\Omega't)})$$
$$+\tfrac{1}{4}b_\perp^2v_{\perp0}[2e^{i\varphi_0}+2e^{i(2\phi_B-\varphi_0)}-2e^{i(\varphi_0-\Omega't)}-e^{i(2\phi_B-\varphi_0-\Omega't)}-e^{i(2\phi_B-\varphi_0+\Omega't)}]+O(b_\perp^3)\}(\hat{\boldsymbol{x}}-i\hat{\boldsymbol{y}})]]\,.\quad(2.22)$$

The nominal pitch-angle cosine μ relative to $\boldsymbol{B}_0$ is defined by $\mu\equiv v_\parallel/v$, and the pitch-angle cosine μ' relative to the background field $\boldsymbol{B}'$ is defined by $\mu'\equiv v'_\parallel/v$. From equations (2.17) and (2.19), we find

$$z(t)=(1-b_\perp^2)v_{\parallel0}\,t+b_\perp v_{\perp0}\,t\sin(\pi/2+\varphi-\phi_B)+(b_\perp v_{\perp0}/\Omega')[\sin(\phi_B-\varphi)-\sin(\Omega't+\phi_B-\varphi)]+(b_\perp^2v_{\parallel0}/\Omega')\sin(\Omega't)+O(b_\perp^3)\,.$$
$$(2.23)$$

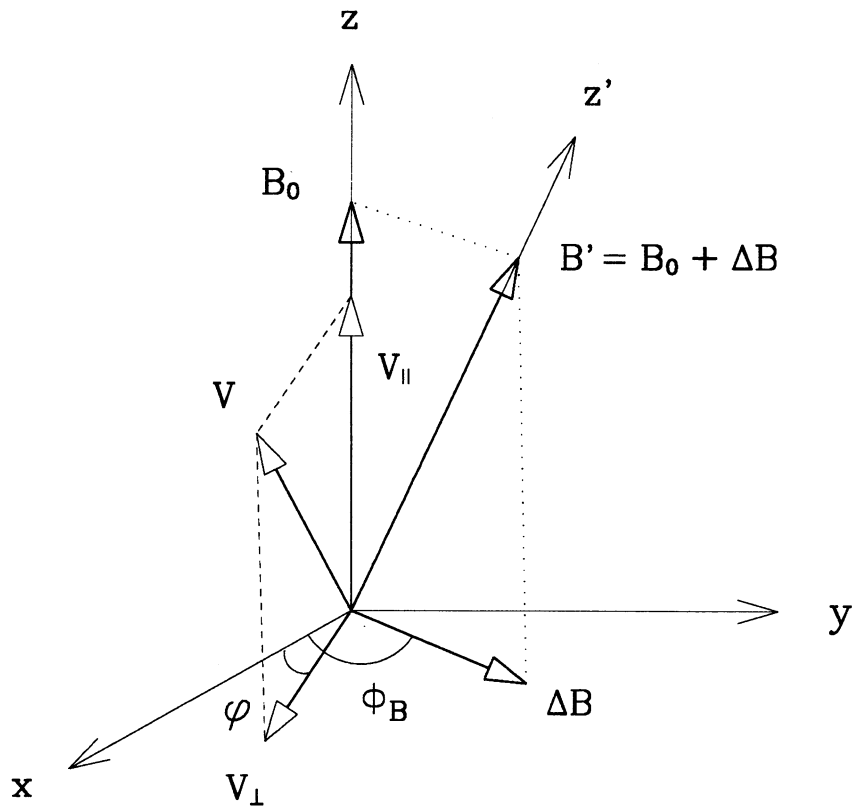

FIG. 2.—Illustration of the coordinate axes used, the velocity and interplanetary magnetic field components, the particle gyrophase φ, and the magnetic field azimuth ϕ_B.

Note that

$$\Omega' = \Omega[1 + \tfrac{1}{2}b_\perp^2 + O(b_\perp^4)] , \tag{2.24}$$

where $\Omega \equiv \Omega_0/\gamma \equiv qB_0/(\gamma mc)$, m is the particle's mass, and Ω_0 is the cyclotron frequency in the mean field B_0.

Now let us consider the effect of the slow fluctuation in B'. The observed normalized standard deviation of field-magnitude fluctuations of $\approx 8\%$ within hour intervals (Denskat & Neubauer 1983) and 2%–10% field-magnitude fluctuation from hour to hour (King 1975) suggest that there exist magnetic "mirrors" separated by $\lesssim 0.014$ AU and characterized by focusing lengths $L_f \equiv |B'(\partial B'/\partial z')^{-1}| \lesssim 0.18$ AU. (The solar wind velocity is ≈ 0.01 AU hr^{-1}.) Since these are much larger than a 10 MeV proton's gyroradius of $\approx 5.4 \times 10^{-4}$ AU in a 5 nT field, in the *absence* of resonant scattering, $\lesssim 10$ MeV protons will conserve their magnetic moments, i.e., $(1 - \mu'^2)/B'$ as energy change is negligible, and adiabatically oscillate between a pair of magnetic mirrors, provided that their μ'-values are small (outside the loss cones). For $\mu' \approx 1$, the change in μ' is negligible. For $\mu' \lesssim 0.3$, the largest μ'-oscillation range is $(-\mu_c', \mu_c')$, where $\mu_c' \approx (\Delta B'/B')^{1/2} \approx 0.28$ independent of particle energy, and $d\mu'/dt \approx v/(2L_f)$. In the presence of counter-streaming medium scale waves, these mirrors are neither permanent nor at rest relative to one another. The associated slow temporal change in B' also adiabatically changes μ', which is not considered above. We also ignore stochastic energy change caused by randomly moving mirrors.

The existence of the μ'-oscillation implies that the particles crisscross the SQLT resonance gap. However, this relatively slow oscillation does not by itself lead to pitch-angle diffusion. Only when resonant waves are present can a particle diffuse from outside the μ'-oscillation range to inside it and continue to diffuse by interacting with different resonant waves as it slowly changes its μ'-value while partaking in the adiabatic oscillation, which takes it across the resonance gap to resonate with another set of resonant waves. In this way, it can access the entire μ' or μ-space. Thus, provided the resonance gap is narrow and the particle crosses the gap quickly, the averaging process for calculating the transport coefficients for small values of μ should include averaging over μ' from $-\mu_c'$ to μ_c'.

Let us estimate the SQLT resonance gap $(-\mu_g', \mu_g')$ and the time it takes the particle to cross the gap. A generous upper bound to the gap is provided by cutting off the $R^{\pm}$ and $L^{\pm}$ wave spectra above the high hydromagnetic wavenumber $|k_{\max}| = 0.3\Omega/v_A$. From the resonance condition in terms of μ', we obtain

$$\mu_g' < \frac{v_A}{b_0 v}\left(\frac{\Omega}{k_{\max} v_A} - 1\right) \approx 2.33 \frac{v_A}{b_0 v} . \tag{2.25}$$

The gap-crossing time is thus $< 4\mu_g'(d\mu'/dt)^{-1}$, which is quite short for $\gtrsim 25$ keV protons. For example, with $v_A = 0.001$ AU hr^{-1}, a 1 MeV (100 keV) proton takes < 0.016 hr (< 0.16 hr) to cross the SQLT resonance gap of width < 0.014 (< 0.046).

From equation (2.20), we see that averaging over φ and ϕ_B effectively averages over μ' from $b_0\mu - b_\perp(1-\mu^2)^{1/2}$ to $b_0\mu + b_\perp(1-\mu^2)^{1/2}$. When we next average over $b_\perp$ from 0 to its maximum value a, say, where $a^2 \ll 1$, for $|\mu| \ll a$, the range of μ' covered becomes $(-a, a)$. The effective averaging μ'-interval is somewhat larger than the maximum μ'-oscillation range $(-a/2^{1/2}, a/2^{1/2})$ implied by the associated B'-variation (see comments after eq. [2.47]) and is much larger than the SQLT resonance gap for $a \gtrsim 0.1$ and $v/v_A \gtrsim 50$.

2.3. *Transport Coefficients*

We now continue our consideration of the coefficients of the transport equation (2.16). To evaluate $\langle\ \rangle_{\tau_{\Omega'}}$, we substitute equations (2.21)–(2.23) (with t replaced by s on the left and by $s - t$ on the right, respectively), into equation (2.16), integrate over s from $s = t$ to $s = t + \tau_{\Omega'}$, and then divide by $\tau_{\Omega'}$. In the final result, we will drop the subscript "0" in $v_{\|0} \equiv v_\|(t)$, $v_{\perp 0} \equiv v_\perp(t)$, and $\varphi_0 \equiv \varphi(t)$. To evaluate $\langle\ \rangle_\Delta$, we average over the magnitude ΔB and azimuth ϕ_B of the medium-scale fluctuation $\Delta\boldsymbol{B}$. We assume the probability distribution of $\Delta\boldsymbol{B}$ is axisymmetric about $\boldsymbol{B}_0$, i.e., independent of ϕ_B. Since $\Delta B/B_0 = b_\perp + O(b_\perp^3)$ and $b_\perp^2 \ll 1$, we will for convenience specify the probability distribution of $b_\perp$ and average over $b_\perp$ instead of over ΔB. In other words, we define $\langle\ \rangle_\Delta \equiv \langle\ \rangle_{\phi_B, b_\perp}$. From equation (2.21), we have trivially

$$\langle v_\| \rangle_{\tau_\Omega, \phi_B, b_\perp, \varphi_0} = (1 - \langle b_\perp^2 \rangle_{b_\perp}) v_{\|0} \,. \tag{2.26}$$

To evaluate the momentum transport coefficients, we use equations (2.2), (2.3), and (2.5) to obtain

$$\begin{aligned}
\delta\boldsymbol{F}[z(t), \boldsymbol{p}(t), t] &= \frac{q}{c} \sum_\sigma \Re \int_{k_1\sigma}^{k_2\sigma} \frac{dk}{2\pi} \exp\,[ikz(t) - i\omega^\sigma(k)t] \delta\bar{B}^\sigma(k) \{[v_\|(t) - w^\sigma(k)](-i\hat{\boldsymbol{x}} + \hat{\boldsymbol{y}}) + iv_\perp(t)\, e^{i\varphi(t)}\hat{\boldsymbol{z}}\} \\
&= \frac{q}{c} \sum_\sigma \Re \int_{k_1\sigma}^{k_2\sigma} \frac{dk}{2\pi} \exp\,[ikz(t) - i\omega^\sigma(k)t + i\varphi(t)] \delta\bar{B}^\sigma(k) \\
&\quad \times \{iw^\sigma(k)[1-\mu^2(t)]^{1/2}\hat{\boldsymbol{p}}(t) - i[v(t) - \mu(t)w^\sigma(k)]\hat{\boldsymbol{\theta}}(t) + [\mu(t)v(t) - w^\sigma(k)]\hat{\boldsymbol{\varphi}}(t)\} \,,
\end{aligned} \tag{2.27}$$

in which the wave phase velocity is denoted by $w^\sigma(k) \equiv \omega^\sigma(k)/k$. The expression in the second form of the above equation is given in spherical polar momentum coordinates (p, θ, φ), with the polar axis parallel to $\boldsymbol{B}_0$, $(\hat{\boldsymbol{p}}, \hat{\boldsymbol{\theta}}, \hat{\boldsymbol{\varphi}})$ the corresponding set of unit vectors, and $\mu \equiv \cos\theta$ the nominal pitch-angle cosine. In going from the Cartesian to the spherical form, we have made use of the relation $\hat{\boldsymbol{x}} + i\hat{\boldsymbol{y}} = e^{i\varphi(t)}\{[1-\mu^2(t)]^{1/2}\hat{\boldsymbol{p}}(t) + \mu(t)\hat{\boldsymbol{\theta}}(t) + i\hat{\boldsymbol{\varphi}}(t)\}$. It is a straightforward matter to reexpress the above in cylindrical momentum coordinates if desired.

Using equation (2.27) and the assumption that waves of different wavenumbers or wave modes are uncorrelated, i.e.,

$$\langle \delta\bar{B}^\sigma(k) \delta\bar{B}^{\sigma'*}(k') \rangle_\delta = (2\pi)^2 I^\sigma(k) \delta_{\sigma\sigma'} \delta(k - k') \,, \tag{2.28}$$

we obtain

$$\begin{aligned}
&\frac{\partial}{\partial \boldsymbol{p}} \cdot \langle \delta\boldsymbol{F}[z(t), \boldsymbol{p}(t), t] \delta\boldsymbol{F}[z(t'), \boldsymbol{p}(t'), t'] \rangle_\delta \cdot \frac{\partial \langle f \rangle_\delta [z(t'), \boldsymbol{p}(t'), t']}{\partial \boldsymbol{p}} \\
&= \frac{1}{2} \frac{q^2}{c^2} \sum_\sigma \Re \int_{k_1\sigma}^{k_2\sigma} dk I^\sigma(k) \exp\,\{i[kz(t) - kz(t') - \omega^\sigma(k)(t' - t) + \varphi(t) - \varphi(t')]\} \\
&\quad \begin{bmatrix} \frac{1}{p^2}\frac{\partial}{\partial p} p^2 & -\frac{1}{p}\frac{\partial}{\partial \mu}[1-\mu^2(t)]^{1/2} & \frac{1}{p[1-\mu^2(t)]^{1/2}}\frac{\partial}{\partial \varphi} \end{bmatrix} \\
&\quad \begin{bmatrix} iw^\sigma(k)[1-\mu^2(t)]^{1/2} & -i[v(t) - \mu(t)w^\sigma(k)] & \mu(t)v(t) - w^\sigma(k) \end{bmatrix}^T \\
&\quad \begin{bmatrix} -iw^\sigma(k)[(1-\mu^2(t')]^{1/2} & i[v(t') - \mu(t')w^\sigma(k)] & \mu(t')v(t') - w^\sigma(k) \end{bmatrix} \\
&\quad \begin{bmatrix} \frac{\partial \langle f \rangle_\delta}{\partial p} & -\frac{[1-\mu^2(t')]^{1/2}}{p(t')}\frac{\partial \langle f \rangle_\delta}{\partial \mu} & \frac{1}{p(t')[1-\mu^2(t')]^{1/2}}\frac{\partial \langle f \rangle_\delta}{\partial \varphi} \end{bmatrix}^T_{t'} \,,
\end{aligned} \tag{2.29}$$

where the brackets denote 1×3 matrices, the superscript T denotes the transpose of a matrix, and the subscript following the last brackets indicates that all time-dependent quantities within are to be evaluated at t'. From equations (2.16), (2.26), and (2.29), we obtain the transport or Fokker-Planck equation:

$$\frac{\partial \langle f \rangle}{\partial t} + (1 - \langle b_\perp^2 \rangle_{b_\perp}) v_\| \frac{\partial \langle f \rangle}{\partial z} = \frac{\partial}{\partial \mu}\left(D_{\mu\mu}\frac{\partial \langle f \rangle}{\partial \mu}\right) + \frac{\partial}{\partial \mu}\left(D_{\mu p}\frac{\partial \langle f \rangle}{\partial p}\right) + \frac{1}{p^2}\frac{\partial}{\partial p}\left[p^2\left(D_{pp}\frac{\partial \langle f \rangle}{\partial p} + D_{p\mu}\frac{\partial \langle f \rangle}{\partial \mu}\right)\right] , \tag{2.30}$$

with the following momentum transport coefficients:

$$\begin{aligned}
D_{\mu\mu} = \frac{1}{2}\frac{q^2}{c^2 p^2} \sum_\sigma \int_{k_1\sigma}^{k_2\sigma} dk I^\sigma(k) \int_0^\infty d\tau \Re \langle \exp\,\{i[kz(t) - kz(t-\tau) - \omega^\sigma(k)\tau + \varphi(t) - \varphi(t-\tau)]\}[1-\mu^2(t)]^{1/2} \\
\times [v - w^\sigma(k)\mu(t)][v - w^\sigma(k)\mu(t-\tau)][1-\mu^2(t-\tau)]^{1/2} \rangle_{\tau_\Omega, \phi_B, b_\perp, \varphi} \,,
\end{aligned} \tag{2.31}$$

$$D_{\mu p} = \frac{1}{2}\frac{q^2}{c^2 p}\sum_\sigma \int_{k_1^\sigma}^{k_2^\sigma} dk I^\sigma(k) \int_0^\infty d\tau \Re\langle \exp\{i[kz(t) - kz(t-\tau) - \omega^\sigma(k)\tau + \varphi(t) - \varphi(t-\tau)]\} \times [1-\mu^2(t)]^{1/2}[v - w^\sigma(k)\mu(t)]w^\sigma(k)[1-\mu^2(t-\tau)]^{1/2}\rangle_{\tau_\Omega,\phi_B,b_\perp,\varphi}, \quad (2.32)$$

$$D_{p\mu} = \frac{1}{2}\frac{q^2}{c^2 p}\sum_\sigma \int_{k_1^\sigma}^{k_2^\sigma} dk I^\sigma(k) \int_0^\infty d\tau \Re\langle \exp\{i[kz(t) - kz(t-\tau) - \omega^\sigma(k)\tau + \varphi(t) - \varphi(t-\tau)]\} \times w^\sigma(k)[1-\mu^2(t)]^{1/2}[1-\mu^2(t-\tau)]^{1/2}[v - w^\sigma(k)\mu(t-\tau)]\rangle_{\tau_\Omega,\phi_B,b_\perp,\varphi}, \quad (2.33)$$

$$D_{pp} = \frac{1}{2}\frac{q^2}{c^2}\sum_\sigma \int_{k_1^\sigma}^{k_2^\sigma} dk I^\sigma(k) \int_0^\infty d\tau \Re\langle \exp\{i[kz(t) - kz(t-\tau) - \omega^\sigma(k)\tau + \varphi(t) - \varphi(t-\tau)]\} \times [w^\sigma(k)]^2[1-\mu^2(t)]^{1/2}[1-\mu^2(t-\tau)]^{1/2}\rangle_{\tau_\Omega,\phi_B,b_\perp,\varphi}. \quad (2.34)$$

In the above derivation, we have made the approximations $p(t-\tau) \approx p(t) \equiv p \equiv p_0$ and $v(t-\tau) \approx v(t) \equiv v \equiv v_0$, since these do not change appreciably in the time interval τ_δ. The derivatives of $\langle f\rangle_\delta[z(t'), \boldsymbol{p}(t'), t']$ in the last line of equation (2.29) have been replaced by their values at $[z(t), \boldsymbol{p}(t), t]$ and moved outside the τ-integral, while their coefficients are kept unmodified in the τ-integral. This approximation is slightly different from the adiabatic approximation as stated in equation (2.16). They are, however, of the same order of accuracy as long as the adiabatic approximation is justified. The upper limit of the τ-integral has been extended from τ_δ to ∞, assuming that the field correlation as seen by the particle falls to negligible values at $\tau > \tau_\delta$. The transport coefficients associated with φ have been omitted, since both $\langle f\rangle$ and the distribution of $\Delta\boldsymbol{B}$ are assumed to be symmetric about $\boldsymbol{B}_0$.

It now remains for us to carry out the integration and averaging indicated in equations (2.31)–(2.34), with appropriate specifications of the probability distribution of $b_\perp$ and making use of the zero-order orbit given in equations (2.21)–(2.23). We shall restrict our attention to the transport coefficient $D_{\mu\mu}$ to demonstrate the significant role of the local background field. Analogous calculations may be performed on the other transport coefficients.

Using the identity

$$e^{iz\sin\theta} = \sum_{n=-\infty}^{\infty} J_n(z)\, e^{in\theta}, \quad (2.35)$$

and the expansion equation (2.23), the factor $\exp\{ik[z(t) - z(t-\tau)]\}$ may be written as a multiple sum over products of Bessel functions $J_n(z)$ and exponentials, and equation (2.31) becomes

$$D_{\mu\mu} = \frac{1}{2}\frac{q^2}{c^2 p^2}\sum_\sigma \int_{k_1^\sigma}^{k_2^\sigma} dk I^\sigma(k) \sum_{l_1}\sum_{l_2}\sum_{l_3}\sum_{l_4}\sum_{l_5} \Re\Big\langle e^{il_1\pi/2}\int_0^\infty d\tau e^{i\tau[kv_\parallel(1-b_\perp^2) - \omega^\sigma(k) - (l_3-l_4)\Omega']} J_{l_1}(kb_\perp v_\perp \tau)$$
$$\times \Big\langle [1-\zeta_\parallel(t)][1-\zeta_\parallel(t-\tau)]v_\perp(t)v_\perp(t-\tau)\exp[i\varphi(t) - i\varphi(t-\tau)]\exp[-i(l_1 - l_2 + l_3)(\varphi - \phi_B)]\exp[-i(l_2 - l_3 + l_4 - l_5)\Omega' t]$$
$$\times J_{l_2}\Big(\frac{b_\perp k v_\perp}{\Omega'}\Big)J_{l_3}\Big(\frac{b_\perp k v_\perp}{\Omega'}\Big)J_{l_4}\Big(\frac{b_\perp^2 k v_\perp}{\Omega'}\Big)J_{l_5}\Big(\frac{b_\perp^2 k v_\perp}{\Omega'}\Big)\Big\rangle_{\tau_{\Omega'},\varphi,\phi_B} + O(b_\perp^3)\Big\rangle_{b_\perp}, \quad (2.36)$$

where $\zeta_{\parallel,\perp}(t) \equiv v_{\parallel,\perp}(t)w^\sigma(k)/v^2$. The combinations $v_\perp(t)v_\perp(t-\tau)\exp[i\varphi(t) - i\varphi(t-\tau)]$ and $[1-\zeta_\parallel(t)][1-\zeta_\parallel(t-\tau)]$ may each be expanded in power of $b_\perp$ up to $b_\perp^2$, then multiplied together and reexpanded up to $b_\perp^2$. The last expansion is substituted in equation (2.36). Averaging the resulting equation over φ and ϕ_B each from 0 to 2π and over t from t to $t + \tau_{\Omega'}$ picks out the nonvanishing terms as those satisfying $l_1 - l_2 + l_3 + n_{\varphi-\phi_B} = 0$ and $l_2 - l_3 + l_4 - l_5 + n_t = 0$, where $n_{\varphi-\phi_B}$ and n_t are constant integers. From this we see that unless $l_4 = l_5 = 0$, the associated terms are of higher order than $b_\perp^2$ and may be neglected. Furthermore, we may replace $J_0(kb_\perp^2 v_\perp/\Omega')\, J_0(kb_\perp^2 v_\perp/\Omega')$ by unity with error $O(b_\perp^4)$. After some lengthy but straightforward algebra, the result may be written as follows:

$$D_{\mu\mu} = \frac{1}{4}\frac{q^2}{c^2 p^2}\sum_\sigma \int_{k_1^\sigma}^{k_2^\sigma} dk I^\sigma(k)[v_\perp^2 R_{\mu\mu}^{\sigma 0} + v_\perp^2 R_{\mu\mu}^{\sigma 1} + v_\perp^2 R_{\mu\mu}^{\sigma 2} + O(b_\perp^3)], \quad (2.37)$$

where the resonance functions $R_{\mu\mu}^{\sigma n}(k; p, \mu)$ are given by

$$v_\perp^2 R_{\mu\mu}^{\sigma 0}(k; p, \mu) = \langle\{(1-\zeta_\parallel)^2[v_\perp J_1(\rho) - b_\perp v_\parallel J_0(\rho)]^2 + [\zeta_\parallel(1-\zeta_\parallel) + (\zeta_\perp/2)^2][b_\perp v_\perp J_0(\rho)]^2 - b_\perp v_\perp^2 \zeta_\perp(1-\zeta_\parallel)J_0(\rho)J_1(\rho)\}\Delta^{\sigma 0}(b_\perp, k, p, \mu)\rangle_{b_\perp}, \quad (2.38)$$

$$v_\perp^2 R_{\mu\mu}^{\sigma 1}(k; p, \mu) = \langle[\{(1-\zeta_\parallel)^2[v_\perp^2 + b_\perp^2(v_\parallel^2 - \tfrac{1}{2}v_\perp^2) + 2v_\parallel\xi - \xi^2] + 2\zeta_\parallel(1-\zeta_\parallel)(2b_\perp^2 v_\perp^2 + \xi^2) + 2\zeta_\perp(1-\zeta_\parallel)v_\perp\xi + \zeta_\perp^2\xi^2\}J_0^2(\rho) + 2(1-\zeta_\parallel)^2 b_\perp v_\perp v_\parallel J_0(\rho)]]\Delta^{\sigma 1}(b_\perp, k, p, \mu)\rangle_{b_\perp}, \quad (2.39)$$

$$v_\perp^2 R_{\mu\mu}^{\sigma 2}(k; p, \mu) = \langle v_\perp^2[(1-\zeta_\parallel)J_1(\rho) + \tfrac{1}{2}b_\perp\zeta_\perp J_0(\rho)]^2\Delta^{\sigma 2}(b_\perp, k, p, \mu)\rangle_{b_\perp}. \quad (2.40)$$

In the above,

$$\zeta_{\parallel,\perp} \equiv v_{\parallel,\perp}w^\sigma(k)/v^2, \qquad \rho \equiv kb_\perp v_\perp/\Omega' = kb_\perp v_\perp/\Omega + O(b_\perp^3),$$
$$\xi \equiv v_\parallel(1-b_\perp^2) - w^\sigma(k) - \Omega'/k = v_\parallel - w^\sigma(k) - \Omega/k - b_\perp^2[v_\parallel + \Omega/(2k)] + O(b_\perp^3),$$

and

$$\Delta^{\sigma n}(b_\perp, k, p, \mu) \equiv \int_{-\infty}^{\infty} d\tau e^{i\{kv_\parallel(1-b_\perp^2)-\omega^\sigma(k)-n\Omega[1+(1/2)b_\perp^2]\}\tau} J_0(kb_\perp v_\perp \tau) \tag{2.41}$$

$$= \frac{2H[\![(kb_\perp v_\perp)^2 - \{kv_\parallel(1-b_\perp^2) - \omega^\sigma(k) - n\Omega[1+(1/2)b_\perp^2]\}^2]\!]}{[\![(kb_\perp v_\perp)^2 - \{kv_\parallel(1-b_\perp^2) - \omega^\sigma(k) - n\Omega[1+(1/2)b_\perp^2]\}^2]\!]^{1/2}}, \tag{2.42}$$

where H is the Heaviside step function. We have combined the τ-integral over $[0, \infty)$ and its complex conjugate into a single real τ-integral over $(-\infty, \infty)$ denoted by $\Delta^{\sigma n}(b_\perp, k, p, \mu)$. We have also made use of the following result (see Luke 1972, p. 486):

$$\int_{-\infty}^{\infty} dt e^{-i\omega t} J_m(t) = 2(-i)^m T_m(\omega)(1-\omega^2)^{-1/2} H(1-\omega^2), \tag{2.43}$$

where T_m denotes the mth degree Chebyshev polynomial of the first kind.

In equations (2.38)–(2.40), the factors $\Delta^{\sigma n}(b_\perp, k, p, \mu)$, $(n = 0, 1, 2)$ contain the $b_\perp$-dependent "broadened" resonant conditions, and $\langle\ \rangle_{b_\perp}$ spreads these resonances over an even wider range of wavenumbers. Thus, $R^{\sigma n}_{\mu\mu}(k; p, \mu)$ incorporates the resonance broadening effect resulting from a statistical distribution of $b_\perp$. It is interesting to note that $b_\perp$ not only modifies the phase of the exponential in the integral that defines $\Delta^{\sigma n}$ (see eq. [2.41]) but also introduces into the integral the factor $J_0(kb_\perp v_\perp \tau)$, which can be traced to the second term in equation (2.23), i.e., to the $(\varphi - \phi_B)$-dependent contribution of $v_\perp$ to the effective parallel velocity. We note also that the presence of $\Delta^{\sigma 1}$ in equation (2.39) implies $|\xi| < b_\perp v_\perp$.

We will not interpret every term in equations (2.38)–(2.40) but will instead indicate in a general way how these resonances may be understood physically. If $b_\perp \neq 0$, the local background field $\boldsymbol{B}'$ is inclined to the direction of the wave normal (which is parallel to $\pm\hat{z}$), and the particle's unperturbed orbit then implies a nonuniform z-motion and a μ-value that oscillates at the gyrofrequency Ω'. The steady component and the various harmonic components of the z-motion give rise to the $n = 1$ cyclotron resonance and the $n \neq 1$ harmonic resonances, respectively. These resonances occur when, in its zero-order orbit, the particle senses field fluctuations at a Doppler-shifted frequency equal to its gyrofrequency or a multiple thereof. Thus, we identify $R^{\sigma n}_{\mu\mu}$, $n = 1, 2$ as resulting from cyclotron resonance and cyclotron harmonic resonance, respectively, between the waves and the energetic particles. For $n = 0$, both transit-time and Landau interactions are included in $R^{\sigma 0}_{\mu\mu}$. Transit-time interaction occurs because the particle tries to conserve its first adiabatic invariant, $(1-\mu'^2)/|\boldsymbol{B}_0 + \Delta\boldsymbol{B} + \delta\boldsymbol{B}|$, in the presence of the fluctuation in magnetic field magnitude, caused by the variation of the relative phase difference between $\delta\boldsymbol{B}$ and $\Delta\boldsymbol{B}$. Note that $\langle\mu\rangle_{\tau_{\Omega'}} = (1-b_\perp^2)^{1/2}\mu'$. Landau resonance occurs because $\delta\boldsymbol{E}$ has a component parallel to the local background $\boldsymbol{B}'$.

Equation (2.41) implies that $\Delta^{\sigma n}(b_\perp, k, p, \mu) \to 2\pi\delta[kv_\parallel - \omega^\sigma(k) - n\Omega]$ as $b_\perp \to 0$. If we let $P(b_\perp) \to \delta(b_\perp)$, where $P(b_\perp)$ denotes the probability distribution of $b_\perp$, then equations (2.38)–(2.40) imply that $R^{\sigma 0}_{\mu\mu}(k; p, \mu) \to 0$, $R^{\sigma 2}_{\mu\mu}(k; p, \mu) \to 0$, and $R^{\sigma 1}_{\mu\mu}(k; p, \mu) \to (1-\zeta_\parallel)^2 2\pi\delta[kv_\parallel - \omega^\sigma(k) - \Omega]$, respectively, and we recover the standard quasi-linear result, i.e., there is only one sharp cyclotron $(n = 1)$ resonance.

At first sight equations (2.38)–(2.40) may suggest that the $n \neq 1$ resonances are negligible relative to the cyclotron resonance, since $v_\perp^2 R^{\sigma n}_{\mu\mu}(k; p, \mu) = O(b_\perp^2)$ for $n = 0, 2$, and $v_\perp^2 R^{\sigma 1}_{\mu\mu}(k; p, \mu) \sim (1-\zeta_\parallel)^2 v_\perp^2 \langle\Delta^{\sigma 1}(b_\perp, k, p, \mu)\rangle_{b_\perp} = O(1)$. However, more careful consideration is necessary, because $v_\perp^2 R^{\sigma n}_{\mu\mu}$ are functions of k, and we should compare them at all relevant values of k, bearing in mind that $D_{\mu\mu}(p, \mu)$ is calculated by integrating the product of $\sum_n v_\perp^2 R^{\sigma n}_{\mu\mu}(k; p, \mu)$ and $I^\sigma(k)$ over k. Except for special values of the parameters, e.g., $v_\perp = 0$, the resonance functions in equations (2.38)–(2.40) do not readily lend themselves to analytical treatment, and we will evaluate $R^{\sigma n}_{\mu\mu}$ and $D_{\mu\mu}$ numerically. To that end, we will transform equations (2.38)–(2.40) to a form suitable for numerical integration over $b_\perp$.

First, we express $\Delta^{\sigma n}(b_\perp, k, p, \mu)$ in terms of the real roots $\pm b_1$ and $\pm b_2$ (or $\pm\alpha_n$, if there are only two real roots) of the biquadratic in $b_\perp^2$ in the argument of the Heaviside function in equation (2.42):

$$\Delta^{\sigma n}(b_\perp, k, p, \mu) = \begin{cases} \dfrac{2H[(b_\perp^2 - b_1^2)(b_2^2 - b_\perp^2)]}{|kv_\parallel + (n/2)\Omega|\,[(b_\perp^2 - b_1^2)(b_2^2 - b_\perp^2)]^{1/2}} & kv_\parallel + \dfrac{n}{2}\Omega \neq 0, \\ \dfrac{2H(b_\perp^2 - \alpha_n^2)}{|k|v_\perp(b_\perp^2 - \alpha_n^2)^{1/2}} & kv_\parallel + \dfrac{n}{2}\Omega = 0, \end{cases} \tag{2.44}$$

where

$$b_{1,2} = \frac{1}{2}\left|\frac{kv_\perp}{kv_\parallel + (n/2)\Omega}\right|\left|\left[1 + 4\,\frac{kv_\parallel + (n/2)\Omega}{kv_\perp}\,\frac{kv_\parallel - \omega^\sigma(k) - n\Omega}{kv_\perp}\right]^{1/2} \mp 1\right|, \tag{2.45}$$

and

$$\alpha_n = [kv_\parallel - \omega^\sigma(k) - n\Omega]/(kv_\perp). \tag{2.46}$$

Second, we need to specify $P(b_\perp)$ in order to evaluate the average $\langle\ \rangle_{b_\perp}$. We choose for simplicity and convenience

$$P(b_\perp) = 2\pi b_\perp \frac{2}{\pi a^2}\left(1 - \frac{b_\perp^2}{a^2}\right)H(a - b_\perp), \tag{2.47}$$

with $0 < a^2 \ll 1$. This $b_\perp$-distribution has a finite range with $\langle b_\perp^2\rangle_{b_\perp}^{1/2} = a/3^{1/2}$. It implies that the normalized magnetic field magnitude B'/B_0 varies in the range $[1, (1-a^2)^{-1/2}]$, with a mean of approximately $1 + a^2/6$. It also implies that both B'/B_0 and

$B'/\langle B'\rangle_{b_\perp}$ have a standard deviation of approximately $a^2/(72)^{1/2}$. For small μ, the maximum μ'-oscillation range $(-\mu_c', \mu_c')$ is given by

$$\mu_c' = a/\sqrt{2}\,. \tag{2.48}$$

Finally, we note that equations (2.38)–(2.40) are of the form $\langle g(b_\perp)\Delta^{\sigma n}(b_\perp, k, p, \mu)\rangle_{b_\perp}$. With the transformation

$$b_\perp^2 = \begin{cases} \frac{1}{2}[b_1^2 + b_2^2 + (b_2^2 - b_1^2)\sin\vartheta] & kv_\parallel + (n/2)\Omega \neq 0\,, \\ \alpha_n^2 + y^2 & kv_\parallel + (n/2)\Omega = 0\,, \end{cases} \tag{2.49}$$

we may rewrite these as follows:

$$\langle g(b_\perp)\Delta^{\sigma n}(b_\perp, k, p, \mu)\rangle_{b_\perp} = \begin{cases} \dfrac{4H(a-b_1)}{a^2\,|\,kv_\parallel + (n/2)\Omega\,|}\displaystyle\int_{-\pi/2}^{\vartheta_u} d\vartheta\left(1 - \frac{b_\perp^2}{a^2}\right)g(b_\perp) & kv_\parallel + \dfrac{n}{2}\Omega \neq 0\,, \\ \dfrac{8H(a-|\alpha_n|)}{a^2\,|kv_\perp|}\displaystyle\int_0^{\sqrt{a^2-\alpha_n^2}} dy\left(1 - \frac{b_\perp^2}{a^2}\right)g(b_\perp) & kv_\parallel + \dfrac{n}{2}\Omega = 0\,, \end{cases} \tag{2.50}$$

where $b_\perp$ is to be substituted from the corresponding lines in equation (2.49), and

$$\vartheta_u = \begin{cases} \pi/2 & 0 \le b_1 < b_2 \le a\,, \\ \sin^{-1}\left(\dfrac{2a^2 - b_1^2 - b_2^2}{b_2^2 - b_1^2}\right) & 0 \le b_1 < a \le b_2\,. \end{cases} \tag{2.51}$$

The integrand in equation (2.50) for each resonance is well behaved, and we are now in a position to numerically evaluate the resonance functions. After the specification of the small-scale wave spectrum $I^\sigma(k)$, we may readily evaluate numerically $D_{\mu\mu}$ in equation (2.31). We will present and discuss the numerical results in the following sections.

3. THE RESONANCE FUNCTIONS

In this and subsequent sections, we will use normalized dimensionless quantities unless noted otherwise. Velocities, frequencies, and time are normalized and rendered dimensionless by dividing by v_A, Ω_0, and Ω_0^{-1}, respectively:

$$\begin{cases} \dfrac{v}{v_A} \to v\,, & \dfrac{\omega^\sigma(k)}{\Omega_0} \to \omega^\sigma(k)\,, & \dfrac{kv_A}{\Omega_0} \to k\,, & \dfrac{D_{\mu\mu}(k; p, \mu)}{\Omega_0} \to D_{\mu\mu}(k; p, \mu)\,, \\ \Omega_0 R_{\mu\mu}^{\sigma n}(k; p, \mu) \to R_{\mu\mu}^{\sigma n}(k; p, \mu)\,, & \Omega_0 t \to t\,. \end{cases} \tag{3.1}$$

Using equations (2.38)–(2.40), (2.50), and (2.51), we calculate the resonance functions for a range of values of the parameters a, μ, v, γ, and for each parallel or antiparallel propagating circularly polarized wave mode. In these calculations, we use the normalized cold plasma dispersion relation (Stix 1962)

$$\omega^\sigma(k) = \pm k(1 + \tfrac{1}{4}k^2)^{1/2} + \tfrac{1}{2}k^2\,, \tag{3.2}$$

where the positive (negative) sign applies for $\sigma = R^+, L^+$ ($\sigma = R^-, L^-$). As remarked in § 2.1, k is restricted to positive (negative) values for $\sigma = R^+, L^-$ ($\sigma = R^-, L^+$). For $|k| \lesssim 0.3$, the cold plasma dispersion relation is reasonably well approximated by the hydromagnetic dispersion relation $\omega^\sigma(k) = \pm k$. The dispersion relations for the L-waves and R-waves are modified at $|k| \gtrsim 1$ and near electron cyclotron frequency, respectively, as a result of thermal damping by plasma protons and electrons (e.g., Miller & Steinacker 1992; Achatz et al. 1993). However, we shall see that the energetic ions in interplanetary space are resonant mainly with waves at $|k| \lesssim 0.3$, and the cold plasma dispersion is adequate for our purpose.

For nonrelativistic particles, we may make the approximation $\gamma = 1$, and $(1 - \mu^2)R_{\mu\mu}^{\sigma n}$ becomes independent of γ. The salient features of the resonance functions predicted by EQLT are illustrated in Figure 3, in which $(1 - \mu^2)2R_{\mu\mu}^{R^+, n}$, ($n = 0, 1, 2$) and their sum $(1 - \mu^2)2R_{\mu\mu}^{R^+} \equiv \sum_n (1 - \mu^2)2R_{\mu\mu}^{R^+, n}$ are displayed *versus* the wavenumber k, for *nominal* values of $\mu = 1, 0.5, 0.2, 0.01$, and -0.2, the other parameters being fixed at $v = 100$, $a = 0.3$, and $\gamma = 1$. If $v_A = 1 \times 10^{-3}$ AU hr^{-1}, a typical value at a heliocentric distance of 1 AU, the normalized velocities $v = 100$ and $v = 1000$ correspond to ~ 100 keV nucleon^{-1} and ~ 10 MeV nucleon^{-1}, respectively. We note that $a = 0.3$ implies $\langle b_\perp\rangle^{1/2} = 0.17$, and that $|\boldsymbol{B}'|/\langle|\boldsymbol{B}'|\rangle_{b_\perp}$, the magnetic field *magnitude* normalized relative to its mean, has a standard deviation of approximately 0.01. These are somewhat smaller than the observed values at 1 AU. To facilitate comparison, in Figure 3, we indicate by a vertical arrow where applicable, the cyclotron resonant wavenumber at which the SQLT delta function is located. We discuss below each resonance function in turn.

3.1. *The $n = 1$ Resonance Function*

From Figure 3, we see that as μ decreases from 1, the range of k-values for which $(1 - \mu^2)R_{\mu\mu}^{R^+, 1} > 0$ broadens and shifts to higher wavenumbers. For the slab model of field fluctuation, SQLT predicts only the $n = 1$ cyclotron resonance:

$$(1 - \mu^2)(R_{\mu\mu}^{R^+, 1})_{\rm SQL} = (1 - \mu^2)(1 - \zeta_\parallel)^2 2\pi\delta[kv_\parallel - \omega^{R^+}(k) - \gamma^{-1}]\,. \tag{3.3}$$

For $v_\parallel = \mu v \gg 1$, (i.e., parallel particle velocity much larger than the Alfvén velocity), the SQLT resonant wavenumber is well approximated by $(k_{\rm res}^{R^+})_{\rm SQL} = [\gamma(v_\parallel - 1)]^{-1}$. With $\sigma = R^+$ in the cold plasma dispersion relation (3.2), SQLT predicts no resonance at $v_\parallel < 3^{3/2}/2$.

When $\mu \lesssim 0.2$, Figure 3 shows that $R_{\mu\mu}^{R^+, 1}$ peaks at an appreciably lower value of k than $(k_{\rm res}^{R^+})_{\rm SQL}$. For example, at $\mu = 0.05$ (not shown in Fig. 3), the FWHM of $(1 - \mu^2)R_{\mu\mu}^{R^+, 1}$ spans from $k = 3.5 \times 10^{-2}$ to $k = 1.1 \times 10^{-1}$, and the peak is at $k_{\rm res}^{R^+, 1} = 5.2 \times 10^{-2}$,

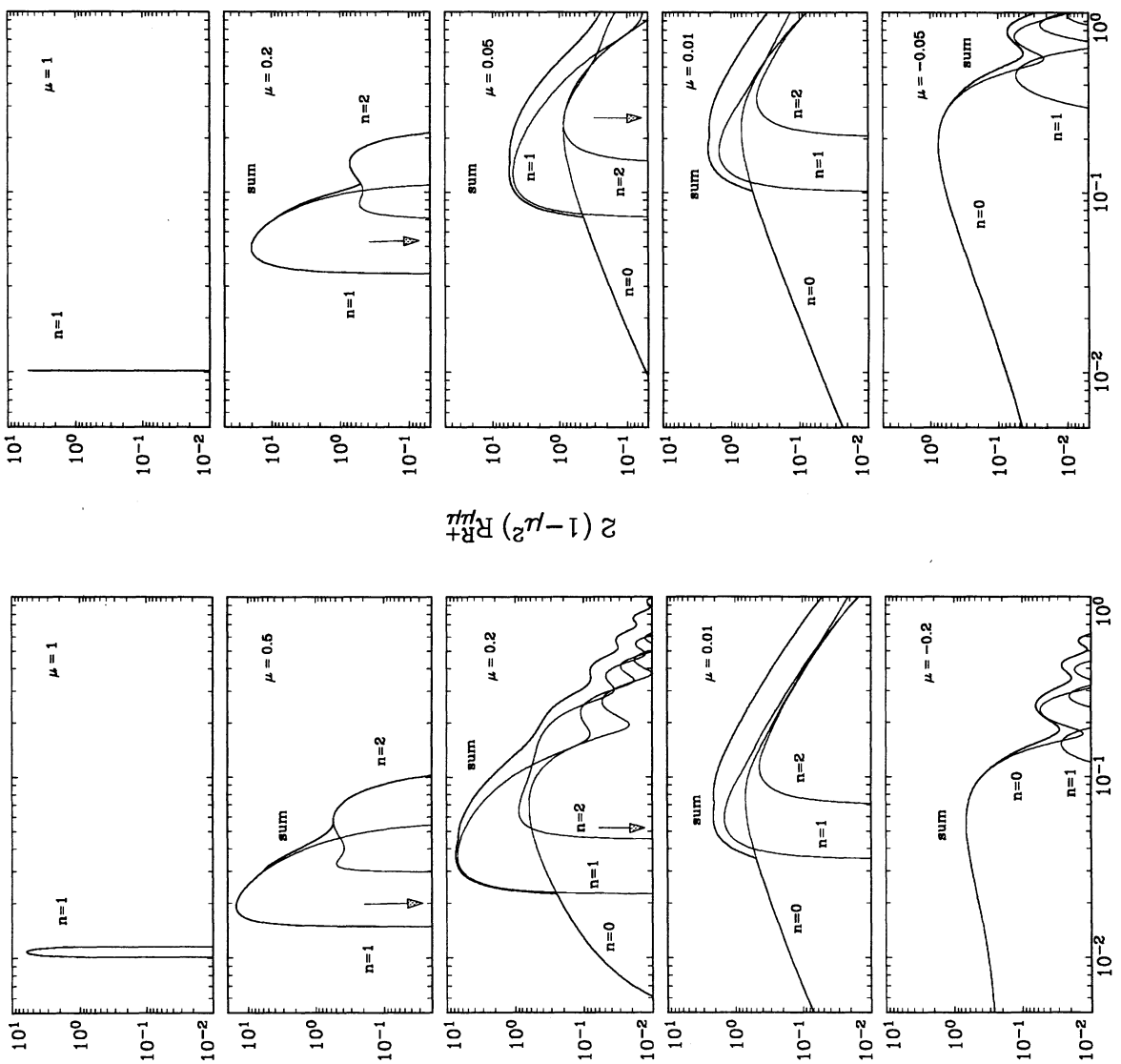

FIG. 3

FIG. 3.—$(1-\mu^2)2R^{R+}_{\mu\mu}$ and its harmonic constituents vs. k for $v = 100$, $\gamma = 1$, and $a = 0.3$

FIG. 4.—Same as Fig. 3, except for $a = 0.1$

FIG. 5.—$(1-\mu^2)2R^{R+}_{\mu\mu}$ and its harmonic constituents vs. k for $a = 0.3$, $\mu v = 1$, and four values of v

FIG. 4

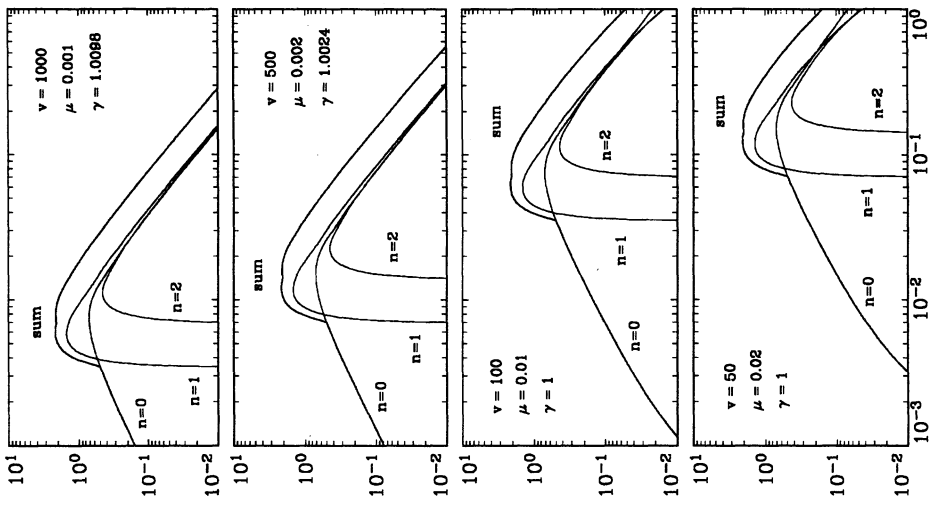

FIG. 5

whereas SQLT predicts a sharp resonance at $(k_{\rm res}^{R+,1})_{\rm SQL} = 2 \times 10^{-1}$. An alternative way of looking at this comparison is as follows. In SQLT, the R^+ waves in the FWHM range of wavenumbers are separately in sharp resonance with particles having a unique value of $\mu = 0.1 \lesssim \mu \lesssim 0.28$; whereas in EQLT, the same waves can all resonate with particles having the *smaller* value of $\mu = 0.05$. In contrast with the SQLT prediction of no resonance at $\mu v < 3^{3/2}/2$ for $\sigma = R+$, Figure 3 shows that in EQLT, the $n = 1$ resonance exists for $\sigma = R+$ even at $\mu v = 1$ with a peak at the *hydromagnetic* wavenumber $k \approx 6 \times 10^{-2}$ and dominates the other two resonance functions at $5 \times 10^{-2} \lesssim k \lesssim 1 \times 10^{-1}$.

3.2. *The $n = 2$ Resonance Function*

The k-range of the $n = 2$ harmonic resonance is located at approximately twice that of the cyclotron resonance at $\mu > 0.7$, but it overlaps with the latter for smaller values of μ. Although the ratio of the peak value of $R_{\mu\mu}^{R+,2}$ to the peak value of $R_{\mu\mu}^{R+,1}$ increases as μ decreases, it is always negligible for the chosen parameters in Figure 3. Since observation suggests that the differential wave intensity $I^{R+}(k)$ falls with increasing k, and $R_{\mu\mu}^{R+,2}$ always peaks at a higher value of k than $R_{\mu\mu}^{R+,1}$, the contribution of the harmonic resonance to $D_{\mu\mu}$ is negligible in comparison to that of the cyclotron resonance.

3.3. *The $n = 0$ Resonance Function*

At $|\mu| \lesssim 0.3$, the $n = 0$ resonance appears over a broad range of wavenumbers and increases in importance relative to the $n = 1$ resonance as μ decreases, dominating the latter at $\mu < 0$. It disappears at $|\mu| \gtrsim 0.3$. An important feature of this resonance function is that it peaks at $k \lesssim 0.08$. However, although it extends to wavenumbers below the range of $n = 1$ resonance, consideration of the spatial scale of medium-scale fluctuation limits the applicable range to wavenumbers $k_{\rm min} \gtrsim 50k_c$ (see § 4).

3.4. *The Effect of the Amplitude of Medium-Scale Fluctuation*

Figure 4 shows the resonance functions $R_{\mu\mu}^{R+,n}$ for $a = 0.1$ and $\mu = 1$, 0.2, 0.05, 0.01, and -0.05, the other parameters being the same as in Figure 3: $v = 100$ and $\gamma = 1$. Comparison of Figures 3 and 4 shows that for the smaller value of a, the resonance functions are narrower at $\mu \gtrsim 0.2$; however, at $\mu \lesssim 0.1$, they are shifted to higher k-values (by a vactor of $\approx 1/a$) and cover a wider k-range (note the logarithmic scale for k). The $n = 0$ resonance for $a = 0.1$ appears only for $|\mu| \lesssim 0.1$. We note that even for $\mu = 0.01$, when the particles are nominally approximately at rest with the forward waves, $R_{\mu\mu}^{R+}$ still peaks at $k < 0.2$, thus allowing the particles to interact with the high wavenumber end of hydromagnetic waves (for convenience, we will refer to $|k| \leq 0.3$ as the *hydromagnetic* range of wavenumbers).

The results here illustrate that as $a \to 0$, the SQLT result is recovered: except for small values of μ, $R_{\mu\mu}^{R+}$ approaches the SQLT delta functions, and at small values of μ, it is shifted to infinite wavenumbers. However, the limit of $a = 0$ does not apply in interplanetary space; already for $a = 0.1$, we have $\langle b_\perp^2 \rangle^{1/2} = 0.058$, and B'/B_0 has a standard deviation of 0.001 (see remarks after eq. [2.47]), figures that are far below observed values at 1 AU. For the L^- waves, SQLT predicts that $(k_{\rm res}^{L-})_{\rm SQL} \gtrsim 1$ for $0 \lesssim \mu \lesssim 1/v$. Thus, with heavy thermal damping of ion-cyclotron waves, SQLT predicts little contribution from L^- waves at $k > 0.3$ to $D_{\mu\mu}$ at $\mu \lesssim 1/v$. However, in EQLT, $R_{\mu\mu}^{L-}$ again peaks at hydromagnetic wavenumbers, allowing these shear Alfvén waves to interact with particles at small values of μ.

3.5. *Variation with Particle Velocity*

We show in Figure 5 $R_{\mu\mu}^{R+}$ *versus* k at $v_\parallel = 1$ for $v = 1000$, 500, 100, and 50, with a fixed at 0.3. (The values of γ are calculated with an assumed value of $v_{\rm A} = 1 \times 10^{-3}$ AU hr^{-1}.) This figure shows that as v decreases, the $R_{\mu\mu}^{R+}$ *versus* k curve shifts horizontally to higher k-values on the log-log plot with only a slight change in shape. The k-shift is by a factor roughly in inverse proportion to v. Note that the resonant range of wavenumbers is widened as they are shifted to the right. Figure 5 suggests that as v decreases below ≈ 20, $R_{\mu\mu}^{R+}$ for $v_\parallel \approx 1$ peaks at increasingly higher values of k. For a steep wave spectrum in the dissipation range (say, power-law index $\lesssim -3$ at $k > 0.2$), this may result in very small values of $D_{\mu\mu}$ for $\mu \sim 1/v$ for $v \lesssim 20$. However, note that this corresponds to very low particle energy (<few keV nucleon^{-1}), to which the present theory does not apply (see later discussion). At sufficiently high energy, the particle gyroradius exceeds the field correlation length (≈ 0.02 AU), and the concept of a medium-scale fluctuation in the background does not apply. However, at such high energies, γ is significantly larger than 1, lowering the resonant wavenumbers and narrowing the resonance gap, which can then be breached by counterstreaming Alfvén waves (Schlickeiser 1989).

The resonance function $R_{\mu\mu}^{L-,n}$ is very similar to $R_{\mu\mu}^{R+,n}$ with a shift toward smaller wavenumbers (see Fig. 1 for the SQLT case), and so we will not exhibit them here. The functions $R_{\mu\mu}^{R-,n}$ and $R_{\mu\mu}^{L+,n}$ can be obtained from $R_{\mu\mu}^{R+,n}$ and $R_{\mu\mu}^{L-,n}$, respectively, with the replacements $\mu \to -\mu$ and $k \to -k$.

3.6. *Summary and Discussion*

To summarize, the resonance function depicted in Figures 3–5 has three interesting and important features: (*a*) the appearance of the $n \neq 1$ resonances, (*b*) the broadening range of resonant wavenumbers as μ decreases, and (*c*) its peaking at a hydromagnetic wavenumber, even at small μ-values, for $v \gtrsim 50$. The last feature implies that the transport of these particles is dominated by interaction with hydromagnetic waves, and the higher frequency ion-cyclotron wave plays only a minor role.

To understand these features, we note that for $b_\perp \neq 0$, a particle executing the unperturbed orbit about the local background $\boldsymbol{B}'$ experiences oscillation in its μ-value at the gyroperiod $\tau_{\Omega'}$ and nonuniform z-motion in the direction of the wave normals, resulting in the appearance of the $n \neq 1$ resonances. Alternatively, the $n \neq 1$ resonances may be understood as resulting from the particle interacting with an oblique wave with second-order compression. Taking into account the particle distribution in nominal gyrophase φ and a statistical distribution of the background $\boldsymbol{B}'$ means averaging over φ, ϕ_B, and $b_\perp$, and this results in a broadened range of resonant wavenumbers. In addition, the mirroring forces set up by the medium-scale B'-variation causes a slow adiabatic μ'-oscillation, which for small values of μ carries the particle back and forth across the SQLT ($n = 1$) resonance gap $(-\mu_g', \mu_g')$.

During this oscillation, the particle resonates with hydromagnetic waves when it is outside the gap and experiences the narrow $n = 0$ resonance within the gap. This means that in calculating $D_{\mu\mu}$, we must average over the μ'-oscillation range $(-\mu_c', \mu_c') = (-a/2^{1/2}, a/2^{1/2})$, which, however, is already covered by the μ'-range $(-a, a)$ spanned by the averaging over φ, ϕ_B, and $b_\perp$. For example, if $v = 100$ and $k_{\max} = 0.3$, the SQLT resonance gap is bounded by $(-0.025, 0.025)$. If $a = 0.3$, the μ'-oscillation range is $(-0.21, 0.21)$, whereas the averaging over φ, ϕ_B, and $b_\perp$ spans the μ'-range $(-0.3, 0.3)$.

We note that no resonance broadening can occur if the μ'-oscillation range is contained in the $n = 1$ resonance gap, i.e., if $\mu_c' < \mu_g'$; in this case, our averaging procedure would make no sense. From equations (2.48) and (2.25), we see that this is so if (in dimensional form)

$$a(1 - a^2)^{1/2} < \frac{\sqrt{2} v_A}{v}\left(\frac{\Omega}{k_{\max} v_A} - 1\right),$$

which does not hold for typical conditions. On the other hand, our averaging procedure is valid only if $\mu_g' \ll \mu_c'$, i.e., if

$$a(1 - a^2)^{1/2} \gg \frac{\sqrt{2} v_A}{v}\left(\frac{\Omega}{k_{\max} v_A} - 1\right).$$

This is well satisfied by, for example, $a = 0.3$, $v/v_A = 100$, and $k_{\max} v_A/\Omega = 0.3$.

4. THE DIFFUSION COEFFICIENT IN μ-SPACE

We now use the resonance functions described in the previous section to calculate $D_{\mu\mu}$ in equation (2.36). We need to specify the wave spectra for the small-scale resonant waves and the applicable wavenumber range $(k_{\min}, k_{\max})$. The correlation length L_c of IMF fluctuation is $\approx 2 \times 10^{-2}$ AU. With typical values of $\Omega \approx 0.5\ s^{-1}$ and $v_A \approx 1 \times 10^{-3}$ AU hr^{-1} at the Earth's orbit, this corresponds to a dimensionless wavenumber $k_c \approx 4 \times 10^{-5}$. We take this as a typical wavenumber for the nonresonant medium-scale fluctuations. Requiring the smallest resonant wavenumber to be sufficiently large so that the integrated wave intensity in the resonant range is an order of magnitude or more smaller than the integrated wave intensity in the medium scale range, we set $k_{\min}$ in the vicinity of 5×10^{-3}, which corresponds to the lowest cyclotron resonant wavenumber for $v = 200$ at $\mu = 1$. Lowering $k_{\min}$ will raise the contribution of the $n = 0$ resonance to $D_{\mu\mu}$.

The computed resonance functions for dimensionless particle velocity v in the range 50–1000 show that they peak at wavenumbers between $\approx 1/v$ and ≈ 0.2 (Fig. 5). To emphasize the effect of wave damping at high wavenumbers, we specify $k_{\max} = 0.3$, i.e., we cut off the wave spectra above $k = 0.3$ for all wave modes. This clearly represents the maximum possible effect of wave damping above this wavenumber. For simplicity, we assume equal differential wave intensities with a Kolmogorov spectrum for all four wavemodes: $I^\sigma(k) = I_0 |k|^{-5/3}$, with k in $(k_{\min}, k_{\max})$ for $\sigma = R^+, L^-$, and in $(-k_{\max}, -k_{\min})$ for $\sigma = R^-, L^+$.

For $v = 100$, $\gamma = 1$, $a = 0.3$, and equal differential wave intensities for the four wave modes, Figure 6 displays the calculated $D_{\mu\mu}$ *versus* μ according to EQLT, and the corresponding SQLT result. The SQLT curve shows at $-0.025 < \mu < 0.025$ a resonance gap that results from the cutoff of the wave spectra at $|k| > 0.3$. In contrast, EQLT predicts no resonance gap, and a minimum value of $D_{\mu\mu}$ at $\mu = 0$ that is about half its maximum value at $\mu = \pm 0.55$. Also shown in Figure 6 are, in the upper panel, the contributions from the $n = 0$, $n = 1$, and $n = 2$ resonances, and in the lower panel, the contributions from the R^+ and L^- waves (both of these possess left helicity, assuming $\hat{z} \cdot \boldsymbol{B}_0 > 0$, and interact with particles in $-0.3 < \mu \leq 1$). We can use the lower panel of Figure 6 to deduce the qualitative features of $D_{\mu\mu}$ when the relative magnitudes of the four differential wave intensities are varied. For example, if only the R^+ and L^- waves are present, then $D_{\mu\mu} = 0$ at $\mu < -0.3$, and a particle with $\mu > -0.3$ initially will not be able to access the μ-range $[-1, -0.3]$. The curves for the R^- and L^+ wave modes are mirror reflections of those for R^+ and L^-, and for clarity, they are not displayed in Figure 6. If only the R^- and L^+ modes (both possessing right helicity if $\hat{z} \cdot \boldsymbol{B}_0 > 0$) are present, then $D_{\mu\mu} = 0$ at $\mu > 0.3$, and a particle with an initial value of $\mu < 0.3$ will not be able to diffuse through wave-particle interaction to $\mu > 0.3$. (However, it can access the region $\mu > 0.3$ through adiabatic focusing in the diverging interplanetary magnetic field). If only R^+ and L^+ waves (with opposite helicities or polarizations and both traveling antisunward) are present in equal intensities, the $D_{\mu\mu}$ will be a factor of ≈ 2 smaller than that in Figure 6. Denskat & Neubauer (1982) reported that $>90\%$ of the interplanetary Alfvén waves are propagating antisunward, and the observations of Matthaeus & Goldstein (1982), Bruno & Dobrowolny (1986), and Valdés-Galicia, Otaola, & Saulés (1993) indicate that the net helicity is small. These observations suggest that we may take $I^{R+}:I^{L+}:I^{R-}:I^{L-} = 1:1:0.1:0.1$. The resulting $D_{\mu\mu}$ is ≈ 0.55 times that shown in Figure 6.

From the upper panel of Figure 6, we see that (*a*) the contribution from the $n = 1$ resonance covers the entire μ-range without a gap; even at $\mu = 0$, this amounts to about 20% of the maximum value of $D_{\mu\mu}$, (*b*) the contribution from the $n = 0$ resonance is only significant at $|\mu| \lesssim 0.25$, and there it is slightly larger than the contribution from the $n = 1$ resonance, and (*c*) the contribution from the $n = 2$ resonance is negligible.

Figure 7 shows $D_{\mu\mu}$ and its various resonance and wave mode constituents for $a = 0.1$, the other parameters being the same as in Figure 6. Even with this small value of a, EQLT still predicts a minimum at $\mu = 1$ that is about a fifth of the maximum. How small must a be for the resonance gap to show up? The answer may be found from Figure 8, which displays $D_{\mu\mu}$ at $\mu = 0$ as a function of a between $a = 0.003$ to $a = 0.3$ and for $v = 50$, 100, and 500. Equal intensities of the four wave modes with a Kolmogorov spectrum cutoff at $k > 0.3$ are assumed as for Figures 6 and 7. (Although $k_{\min}$ has been chosen to be slightly lower for $v = 500$, the $D_{\mu\mu}$ curve actually differs insignificantly when the larger value of $k_{\min} = 0.002$ is used). We see that for $v = 500$, $D_{\mu\mu}$ at $\mu = 0$ decreases continuously by a factor of 40 as a decreases from 0.3 to 0.003. Since a is probably not smaller than 0.1 for typical interplanetary conditions, no resonance gap exists for protons with this nominal energy of ≈ 2.5 MeV. For $v = 50$ and $v = 100$, corresponding to nominal proton energies of ≈ 25 keV and ≈ 100 keV, respectively, $D_{\mu\mu}$ $(\mu = 0)$ falls steeply to zero only when a decreases below 0.03 and 0.015, respectively. Thus, even for these low-energy protons, the resonance gap does not exist.

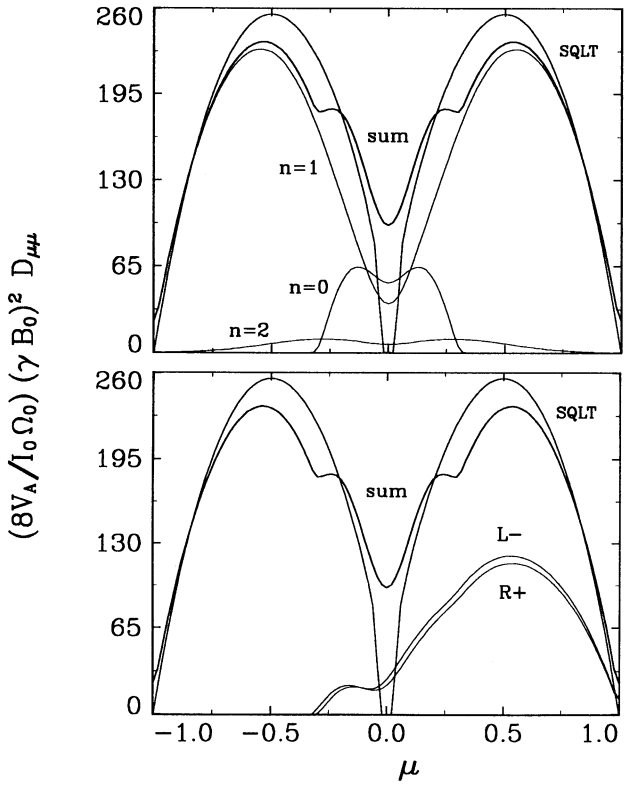

FIG. 6

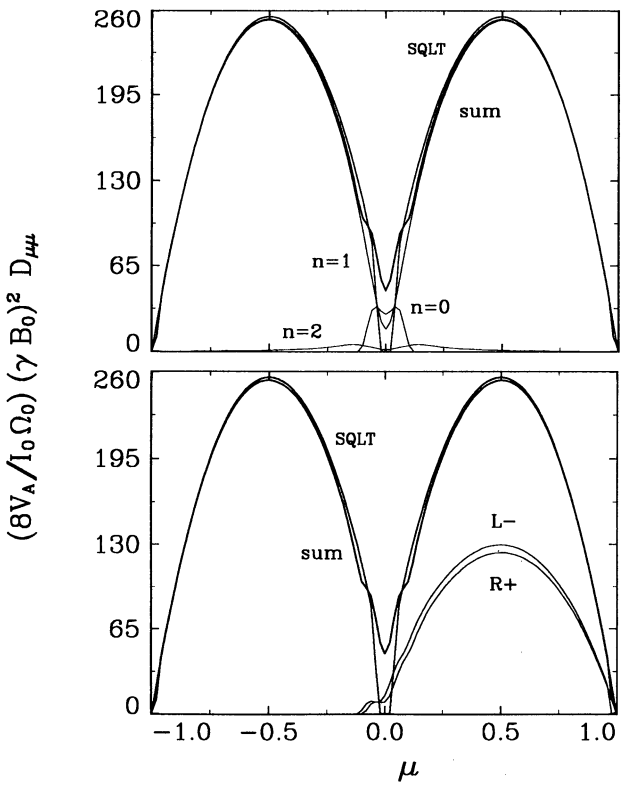

FIG. 7

FIG. 6.—$D_{\mu\mu}$ vs. μ for $v = 100$ and $a = 0.3$. *Top*: the $n = 0$, $n = 1$, and $n = 2$ harmonic contributions. The SQLT result with the resonance gap is also shown for comparison. *Bottom*: The contribution to $D_{\mu\mu}$ from the L^- and R^+ waves; the curve for the L^+ and R^- waves are mirror reflections about $\mu = 0$ of the curves for L^- and R^+ waves, respectively. Equal differential wave intensities are assumed: $I^{\sigma}(k) = I_0 |k|^{-5/3}$ for $0.005 < |k| < 0.3$, and $I^{\sigma}(k) = 0$, otherwise, for all σ-modes.

FIG. 7.—Same as Fig. 6, except that $a = 0.1$

The variation of the mean free path λ with v for nonrelativistic protons ($\gamma \approx 1$) as calculated using EQLT is illustrated in Figure 9 for $a = 0.05$, 0.1, and 0.3. The mean free path here is defined by the (dimensioned) equation (Earl 1974)

$$\lambda = \frac{3}{8} v \int_{-1}^{1} d\mu \frac{(1 - \mu^2)^2}{D_{\mu\mu}} . \tag{4.1}$$

Figure 9 shows that for $a = 0.3$, λ increases by a factor of ≈ 3 when v/v_A increases from 25 to 800. If we take $v_A = 1 \times 10^{-3}$ AU hr^{-1}, this corresponds to an increase of proton rigidity from ≈ 10 MV to ≈ 300 MV. This variation of λ with velocity or rigidity for nonrelativistic particles is qualitatively similar to the prediction of SQLT in the absence of wave dissipation. When the effect of EQLT resonance broadening is reduced by decreasing a to 0.1 and 0.05, λ turns up as v/v_A falls below ≈ 50 and ≈ 100, respectively. This is the result of the cutoff in the wave spectra above $|k| = 0.3$. Since this cutoff is deliberately set to overestimate the effect of

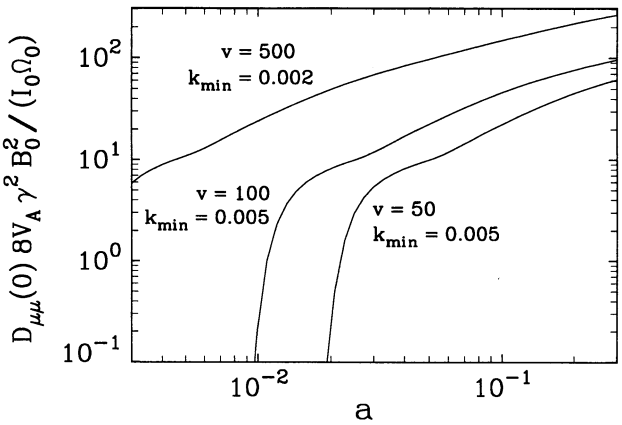

FIG. 8

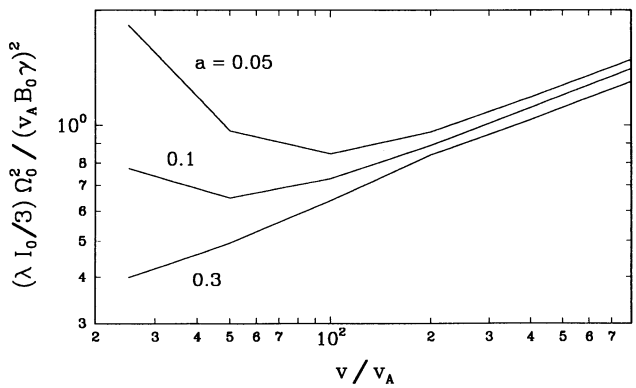

FIG. 9

FIG. 8.—$D_{\mu\mu}$ ($\mu = 0$) vs. a, for (*a*) $v = 50$, $k_{min} = 0.005$, (*b*) $v = 100$, $k_{min} = 0.005$, and (*c*) $v = 500$, $k_{min} = 0.002$

FIG. 9.—The scattering mean free path λ vs. particle velocity v; $a = 0.05$, 0.1, and 0.3

steepened wave spectra in the dissipation range, the actual turnup should occur at much lower rigidities. We note that λ is inversely proportional to the wave intensity level I_0, which is subject to large uncertainty.

5. SUMMARY AND DISCUSSION

Recent works that take into account the steepening of the IMF fluctuation spectrum in the dissipation range (Smith et al. 1990) and/or the effects of thermal damping (Davila & Scott 1984a, b; Miller & Steinacker 1992; Achatz et al. 1993) show that SQLT predicts, contrary to SEP observation, very large or infinite scattering mean free paths despite the inclusion of counterstreaming waves. In this paper, we have presented EQLT, a heuristic extension of SQLT, to take account of the medium-scale fluctuation in the background IMF, by averaging over the background field direction and magnitude. Our approach roughly follows the nonlinear theories of Jones et al. (1978) and Völk (1975), but keeping the quasi-linear treatment, and using the cold plasma dispersion relation for parallel and antiparallel $R^{\pm}$ and $L^{\pm}$ waves.

The main conclusion from EQLT is that the medium-scale fluctuation significantly broadens the wave-particle resonance function at small values of $|\mu|$, allowing SEP with energies down to ≈ 25 keV nucleon^{-1} to resonate with hydromagnetic waves at all pitch angles, thus removing the SQLT resonance gap. The result here probably represents an underestimate, because IMF observation indicates that the parameter a is likely to be larger than 0.3, the largest value used in our calculations. However, much larger values of a would require a full nonlinear treatment. Our results are qualitatively consistent with the nonlinear results of Jones et al. (1978) and Kaiser et al. (1978). A quantitative comparison between their results and ours is not possible because we consider lower rigidities and a superposition of traveling waves.

The main assumption in EQLT are as follows:

1. The IMF fluctuations can be divided into a nonresonant component $\Delta \boldsymbol{B}$ of medium spatial scale and a resonant component $\delta \boldsymbol{B}$ of small-scale, and $\delta B \ll \Delta B \ll B_0$.
2. The resonant fluctuation is described by the slab model consisting of plane cold plasma waves propagating parallel and antiparallel to $\boldsymbol{B}_0$.
3. The medium-scale component $\Delta \boldsymbol{B}$ is described by an axially symmetric probability distribution.
4. The perturbation to the particle momentum caused by wave-particle interaction may be calculated using the zero-order unperturbed orbit about the constant background magnetic field $\boldsymbol{B}'$.
5. The particle undergoes adiabatic μ'-oscillation as a result of the medium-scale variation of $|\boldsymbol{B}'|$, allowing particles with $\mu' \ll 1$ to oscillate across the SQLT resonance gap.

If we take the observed correlation length $L_c \approx 3 \times 10^{-2}$ AU of IMF fluctuations as the length scale of ΔB (corresponding to the dimensionless wavenumber $k_c \approx 2 \times 10^{-5}$ at heliocentric distance $r = 1$ AU), then for a clear separation of the length scales and amplitudes of $\delta \boldsymbol{B}$ and $\Delta \boldsymbol{B}$, we would require the resonant waves to have a minimum wavenumber $k_{\min} \gtrsim 1 \times 10^{-3}$. However, it is only at *small* values of μ that we require EQLT to modify the SQLT prediction of a resonance gap, and from Figure 5 (in which $\mu v = 1$ for all panels) we estimate that the above requirement is satisfied for $v \lesssim 1500$, i.e., for $\lesssim 20$ MeV nucleon^{-1} SEP. Since v_A is approximately $\propto 1/r$, this maximum energy is larger at smaller heliocentric distance r. The above upper energy limit is to satisfy the assumption of separation of length scales in EQLT and does not at all imply that the resonance gap exists at higher energy. Quite the contrary, since Figure 5 shows that the resonant wavenumbers are in the hydromagnetic range for $v = 1000$ and $\mu = 0.001$, increasing either μ or v from these values will simply lower the resonant wavenumbers *away* from the dissipation range. In fact, with increasing particle energy the SQLT resonant gap narrows and eventually disappears (at $\gamma \gtrsim 2$) in the presence of counterstreaming Alfvén waves (Achatz et al. 1993), and there is no need to improve on SQLT at high particle energies.

The magnitude of $D_{\mu\mu}$ at small values of $|\mu|$ has important implications for understanding particle acceleration by a traveling interplanetary shock, for it controls the rate at which particles are scattered back to the shock for further acceleration (Lee 1983; Lee & Ryan 1986; Reames 1990, 1993, 1994). Ng & Reames (1994) showed that streaming SEP of sufficient intensity can excite the ambient outward R^+ and L^+ waves to grow by greater than an order of magnitude within a few hours at $\lesssim 0.3$ AU heliocentric distance. Streaming ($\mu \approx 1$) low-energy protons of ≈ 25 keV ($v = 50$) have been observed to excite hydrodynamic waves at wavenumbers down to $k \approx 2 \times 10^{-2}$ in front of traveling interplanetary shocks (e.g., Lee 1983; Tan et al. 1989). In SQLT, these wavenumbers are too low to allow the excited waves to resonantly scatter high-energy protons with $|\mu| \approx 0$. However, because of the resonance broadening in EQLT (Fig. 5), these waves can now scatter higher energy protons of $\lesssim 10$ MeV ($v \lesssim 1000$) across $\mu \approx 0$, thus increasing the efficiency of the shock acceleration process.

There are, of course, many other treatments of resonance broadening. Nonlinear resonance broadening is discussed in e.g., Völk (1975) and Fisk (1979). We discuss briefly two recent approaches to resonance broadening below. Schlickeiser & Achatz (1993a, b) derived the resonance function broadened by the thermal damping of ion-cyclotron waves (Krommes 1984):

$$R^{\sigma}(k_{\parallel}) = \Gamma^{\sigma}(k_{\parallel})/[\Gamma^{\sigma}(k_{\parallel})^2 + (v_{\parallel} k_{\parallel} + \Omega_0 - \omega^{\sigma})^2] ,$$

where $\Gamma^{\sigma}(k_{\parallel})$ denotes the damping rate of the σ-mode wave at the parallel wavenumber $k_{\parallel}$. In the wave turbulence model, they obtained relatively small nonzero values of $D_{\mu\mu}$ at $\mu \approx 0$, and electron and proton mean free paths in agreement with Palmer (1982). In a different approach, Bieber & Matthaeus (1991) and Bieber et al. (1994) introduced via the concept of dynamical turbulence a different resonance function, which may be formally obtained from the above equation by the replacement $\Gamma^{\sigma} \rightarrow \alpha k_{\parallel} v_A$, where α is a parameter that describes the strength of dynamical damping. Bieber et al. (1994) also proposed another resonance function via a random sweeping model of dynamical turbulence, from which they calculated proton and electron mean free paths as a function of rigidities. The dynamical turbulence model was also studied in Schlickeiser & Achatz (1993a, b). We note that thermal wave damping, dynamical turbulence, and medium-scale IMF fluctuations all imply broadening of the resonance function; the last appears to be the most effective.

In this paper, we have adopted the slab turbulence geometry for simplicity (note, however, that the wavevector is not parallel to the local background $\boldsymbol{B}'$). Would a different turbulence geometry alter our conclusion? The resonance broadening in EQLT is due principally to averaging over the particle distribution in nominal gyrophase and over a statistical distribution of the background $\boldsymbol{B}'$. This averaging spans the μ'-oscillation resulting from the medium-scale adiabatic variation in $|\boldsymbol{B}'|$. So long as the background magnetic field varies in direction and magnitude beyond the resonant scales, this mode of resonance broadening will be present and EQLT should increase back-scattering in other turbulence geometries as well. On the other hand, it has been shown that scattering near $\mu = 0$ can be reduced by invoking oblique Alfvén waves (Lee & Völk 1975; Jaekel & Schlickeiser 1992) or two-dimensional turbulence (Bieber et al. 1994). It appears that these latter approaches may be combined with the resonance broadening discussed in this paper to yield transport coefficients in accord with SEP observation.

It is a pleasure to thank L. M. Barbier, F. C. Jones, and J. M. Miller for discussion. We are indebted to the referee for valuable comments.

REFERENCES

Achatz, U., Dröge, W., Schlickeiser, R., & Wibberenz, G. 1993, J. Geophys. Res., 98, 13261
Achatz, U., Steinacker, J., & Schlickeiser, R. 1991, A&A, 250, 266
Bieber, J. W., & Matthaeus, W. H. 1991, Proc. 22nd Int. Cosmic-Ray Conf. (Dublin), 3, 248
Bieber, J. W., Matthaeus, W. H., Smith, C. W., Wanner, W., Kallenrode, M.-B., & Wibberenz, G. 1994, ApJ, 420, 294
Bruno, R., & Dobrowolny, M. 1986, Ann, Geophys., 4, A-17
Davila, J. M., & Scott, J. S. 1984a, ApJ, 280, 334
———. 1984b, ApJ, 285, 400
Denskat, K. U., & Neubauer, F. M. 1982, J. Geophys. Res., 87, 2215
———. 1983, in Solar Wind Five, ed. M. Neugebauer (NASA CP-2280), 81
Earl, J. A. 1974, ApJ, 193, 231
Fisk, L. A. 1979, in Solar System Plasma Physics, ed. E. N. Parker, C. F. Kennel, & L. J. Lanzerotti, Vol. 1 (New York: North-Holland), 177
Goldstein, M. L. 1976, ApJ, 204, 900
Hall, D. E., & Sturrock, P. A. 1967, Phys. Fluids, 10, 2620
Jaekel, U., & Schlickeiser, R. 1992, J. Phys. G. Nucl. Part. Phys., 18, 1089
Jones, F. C., Birmingham, T. J., & Kaiser, T. B. 1978, Phys. Fluids, 21, 347
Jones, F. C., Kaiser, T. B., & Birmingham, T. J. 1973, Phys. Rev. Lett., 31, 485
Kaiser, T. B., Birmingham, T. J., & Jones, F. C. 1978, Phys. Fluids, 21, 361
Kennel, C. F., & Engelmann, F. 1966, Phys. Fluids, 9, 2377
King, J. H. 1975, Interplanetary Magnetic Field Data Books, NASA/NSSDC Publ. 75-04
Klimas, A. J., & Sandri, G. 1971, ApJ, 169, 41
Krommes, J. A. 1984, in Basic Plasma Physics, ed. A. A. Galeev & R. N. Sudan, Vol. 2 (New York: North-Holland), 183
Kulsrud, R. M., & Pearce, W. P. 1969, ApJ, 156, 445
Lee, M. A. 1983, J. Geophys. Res., 88, 6109
Lee, M. A., & Ryan, J. M. 1986, ApJ, 303, 829
Lee, M. A., & Völk, H. J. 1975, ApJ, 198, 485
Luke, Y. L. 1972, in Handbook of Mathematical Functions, ed. M. Abramowitz & I. A. Stegun (New York: Dover), 479
Matthaeus, W. H., & Goldstein, M. L. 1982, J. Geophys. Res., 87, 6011
Miller, J. A., & Steinacker, J. 1992, ApJ, 399, 284
Ng, C. K., & Reames, D. V. 1994, ApJ, 424, 1032
Palmer, I. D. 1982, Rev. Geophys. Space Phys., 20, 335
Reames, D. V. 1990, ApJ, 358, L63
———. 1993, Adv. Space Res., 13, 331
———. 1994, in Proc. 3rd SOHO workshop, ed. A. Poland (ESA SP-373), 107
Roberts, D. A., Goldstein, M. L., & Klein, W. L. 1990, J. Geophys. Res., 95, 4203
Schlickeiser, R. 1989, ApJ, 336, 243
———. 1992, in Particle Acceleration in Cosmic Plasmas, ed. G. P. Zank & T. K. Gaiser (New York: AIP), 92
Schlickeiser, R., & Achatz, U. 1993a, J. Plasma Phys., 49, 63
———. 1993b, J. Plasma Phys., 50, 85
Smith, C. W., Bieber, J. W., & Matthaeus, W. H. 1990, ApJ, 363, 283
Steinacker, J., & Miller, J. A. 1992, ApJ, 393, 764
Stix, T. H. 1962, The Theory of Plasma Waves (New York: McGraw-Hill)
Tan, L. C., Mason, G. M., Gloeckler, G., & Ipavich, F. M. 1989, J. Geophys. Res., 98, 21077
Völk, H. J. 1973, Ap&SS, 25, 471
———.1975, Rev. Geophys. Space Phys., 13, 4